

Angular bispectrum and trispectrum of scalar-induced gravitational waves: all contributions from primordial non-Gaussianity f_{NL} and g_{NL}

Jun-Peng Li,^{a,b} Sai Wang^{1, a}, Zhi-Chao Zhao,^c Kazunori Kohri^{d,e,f}

^aTheoretical Physics Division, Institute of High Energy Physics, Chinese Academy of Sciences, 19B Yuquan Road, Shijingshan District, Beijing 100049, China

^bSchool of Physics, University of Chinese Academy of Sciences, 19A Yuquan Road, Shijingshan District, Beijing 100049, China

^cDepartment of Applied Physics, College of Science, China Agricultural University, 17 Qinghua East Road, Haidian District, Beijing 100083, China

^dDivision of Science, National Astronomical Observatory of Japan (NAOJ), and SOKENDAI, 2-21-1 Osawa, Mitaka, Tokyo 181-8588, Japan

^eTheory Center, IPNS, and QUP (WPI), KEK, 1-1 Oho, Tsukuba, Ibaraki 305-0801, Japan

^fKavli IPMU (WPI), UTIAS, The University of Tokyo, Kashiwa, Chiba 277-8583, Japan

E-mail: lijunpeng@ihep.ac.cn, wangsai@ihep.ac.cn, zhaozc@cau.edu.cn, kohri@post.kek.jp

Abstract. Studying the primordial non-Gaussianity of inflationary perturbations is crucial for testing the inflation paradigm of the early universe. In this work, we conduct a comprehensive analysis of the angular bispectrum and trispectrum of scalar-induced gravitational waves (SIGWs) in the presence of local-type primordial non-Gaussianity parameterized by f_{NL} and g_{NL} , deriving their semi-analytical formulae for the first time. Our findings indicate that it is the presence of primordial non-Gaussianity that leads to a non-Gaussian SIGW background, suggesting that the angular bispectrum and trispectrum of SIGWs could serve as probes of the primordial non-Gaussianity. Our numerical results further illustrate that f_{NL} and g_{NL} exert significant impacts on the spectral amplitudes, potentially reaching up to 10^{-5} for the former and 10^{-8} for the latter. In particular, we demonstrate that the angular bispectrum and trispectrum exhibit characteristic dependence on the angular multipoles and frequency bands. They hold potentials to be measured by gravitational-wave detectors that may advance our understanding of the origin of the universe.

¹Corresponding author

Contents

1	Introduction	1
2	Effects of primordial non-Gaussianity on the SIGW energy density	3
3	Angular correlation functions	5
4	Semi-analytic formulae for angular bispectrum and trispectrum	7
4.1	Angular bispectrum	13
4.2	Angular trispectrum	14
4.3	Frequency and multipole dependence	15
5	Numerical results	16
5.1	Angular bispectrum	16
5.2	Angular trispectrum	18
6	Discussion and Conclusion	20

1 Introduction

Primordial non-Gaussianity stands for the deviation from Gaussian distribution of the primordial curvature perturbations, thus characterizing the dynamics of the early universe during inflation [1–7]. Though the standard inflation paradigm predicts the nearly Gaussian perturbations [8, 9], many other inflation models hold no brief for this prediction [10]. In particular, the primordial bispectrum is characterized by an amplitude parameter f_{NL} , while the primordial trispectrum by g_{NL} and so on [11]. Constraints on the primordial non-Gaussianity have been obtained through observations of cosmic microwave background (CMB) [12] and large-scale structure (LSS) [13, 14]. However, these observations are only responsive to the cosmological perturbations on large scales that are comparable to the overall observational patch of the universe, leaving the perturbations on smaller scales to be insensitive. Since modes of smaller wavelength reentered the horizon earlier, the universe before the last-scattering surface would have been opaque to the electromagnetic probes [15]. Therefore, to conquer the above challenge, it is necessary to develop alternative probes that can effectively convey information from the early universe to our detectors. Given that Einstein’s general relativity predicts that gravitational waves (GWs) propagate without dissipation [16, 17], we expect them to be a valuable new messenger of the early universe on small scales, in contrast to the traditional observations such as CMB and LSS on large scales.

The scalar-induced gravitational waves (SIGWs) are sensitive to the local-type primordial non-Gaussianity on small scales, making them potential indicators of this non-Gaussianity. Theoretically, they were produced through non-linear processes by the linear inflationary perturbations that reentered the Hubble horizon in the early universe [18–24]. Taking into account f_{NL} and g_{NL} can lead to significant alterations by several orders of

magnitude in both the energy-density fraction spectrum and the angular power spectrum [25], especially within the projected sensitivity regimes of future or futuristic gravitational-wave detection programs [26–50]. This suggests the potential for measuring primordial non-Gaussianity through the search for an anisotropic SIGW background. Other related works can be found in Refs. [51–69] and Refs. [70–72], respectively. Additionally, in conjunction with the production of scalar-induced gravitational waves, these scalar perturbations may gravitationally collapse into primordial black holes (PBHs) [73, 74], which are believed to be a reasonable candidate for cold dark matter (e.g., see review in Ref. [75, 76]). The characteristic mass function of PBHs can also be significantly altered due to presence of the primordial non-Gaussianity [51, 52, 77–102].

Higher-order statistics of the energy-density perturbations, the angular bispectrum and trispectrum in particular, characterize the non-Gaussianity of SIGW background. While the angular power spectrum is a Fourier counterpart of the two-point correlator, the angular bispectrum and trispectrum correspond to the three- and four-point correlators, which are a natural extrapolation of skewness and kurtosis for a random variable. They would be highly valuable in extracting additional physical information about inflation, serving as another means to probe the primordial non-Gaussianity. It is reasonably anticipated that GW background produced by the Gaussian inflationary perturbations is also Gaussian. Conversely, the non-Gaussianity of SIGW background can result from non-Gaussian inflationary perturbations, indicating that non-vanishing angular bispectrum and trispectrum would be a smoking gun of the primordial non-Gaussianity. Recently, the angular bispectrum of a generic cosmological GW background has been investigated in Refs. [103, 104], while the study about angular trispectrum of GW background remains a blank. Additional studies on the non-Gaussianity of SIGWs are available in Refs. [105–109]. Moreover, the angular bispectrum of SIGWs has been evaluated for the first time in Ref. [70], though only f_{NL} was crudely taken into account.

In this work, we will perform a comprehensive analysis of the angular bispectrum and trispectrum of SIGWs by simultaneously taking into account the local-type primordial non-Gaussianity parameterized by f_{NL} and g_{NL} . Following a diagrammatic approach [25], we will study the non-Gaussianity of SIGW background via including higher-order energy-density perturbations in SIGWs. We will derive semi-analytic formulae for the angular bispectrum and trispectrum and further find the consistency relations between them with the angular power spectrum, respectively. In a numerical manner, we will demonstrate significant influence of the primordial non-Gaussianity on both their spectral amplitudes and profiles. Moreover, we will prove the non-vanishing angular bispectrum or trispectrum of SIGWs to be a smoking gun of the primordial non-Gaussianity. We wish this work to lay a solid foundation for observational studies of the early-universe physics with the cutting-edge GW probe, complementing other traditional probes such as CMB, LSS, and so on.

The paper is organized as follows. We briefly review the energy-density fraction spectrum of SIGWs in Section 2. We introduce the angular correlation functions of the density contrasts of SIGWs in Section 3. We derive the semi-analytic formulae for the angular bispectrum and trispectrum of SIGWs in Section 4, and demonstrate the corresponding numerical results in Section 5. Conclusions and discussion are shown in Section 6.

2 Effects of primordial non-Gaussianity on the SIGW energy density

The SIGW background arises from the non-linear interactions of primordial curvature perturbations, with the primordial non-Gaussianity anticipated to leave significant imprints on it. Apart from the alteration of the averaged energy density spectrum, the specific shape of primordial non-Gaussianity that stands for the coupling between long- and short- wavelength curvature perturbations modulates the distribution of SIGWs. This modulation creates inhomogeneities on large scales, resulting in an anisotropic SIGW background in observations. Furthermore, this modulation also inevitably causes a departure from Gaussian statistic in the SIGW background, which can be described by the angular bispectrum and trispectrum, etc.

First of all, we will review the impacts of the statistics of primordial curvature perturbations, denoted as ζ , on the energy-density fraction spectrum of SIGWs. Schematically, the strain of SIGWs can be represented as $h_{ij} \sim \zeta^2$ [18–21], and the corresponding energy density on subhorizon scales is expressed in terms of a four-point correlator of ζ , i.e., $\rho_{\text{gw}} \sim h_{ij,l}h_{ij,l} \sim \zeta^4$. Therefore, both the bispectrum and trispectrum of ζ can contribute to it. In this work, we focus on the local-type primordial non-Gaussianity characterized by f_{NL} and g_{NL} . At a spatial location \mathbf{x} , we express ζ in terms of their Gaussian components ζ_g , namely, [11, 110, 111]

$$\zeta(\mathbf{x}) = \zeta_g(\mathbf{x}) + \frac{3}{5}f_{\text{NL}} \left[\zeta_g^2(\mathbf{x}) - \langle \zeta_g^2(\mathbf{x}) \rangle \right] + \frac{9}{25}g_{\text{NL}}\zeta_g^3(\mathbf{x}) , \quad (2.1)$$

where the angle brackets stand for an ensemble average. Though f_{NL} and g_{NL} are scale-independent, our work can be readily extended to a scale-dependent case, which is left to our future works. Using Eq. 2.1, the multi-point correlators of ζ can be contracted as the sum of two-point correlator of ζ_g . For example, the leading order of the primordial curvature bispectrum can be expressed as $\mathcal{O}(f_{\text{NL}})\langle \zeta_g^2 \rangle^2$, and the trispectrum as $\mathcal{O}(f_{\text{NL}}^2)\langle \zeta_g^2 \rangle^3 + \mathcal{O}(g_{\text{NL}})\langle \zeta_g^2 \rangle^3$. We further decompose ζ_g into short-wavelength modes ζ_{gS} and long-wavelength modes ζ_{gL} , i.e., [112]

$$\zeta_g = \zeta_{gS} + \zeta_{gL} . \quad (2.2)$$

Considering Eqs. (2.1,2.2), we can express the four-point correlator of ζ in terms of f_{NL} , g_{NL} , and the dimensionless power spectra of ζ_{gX} defined as

$$\langle \zeta_{gX}(\mathbf{q})\zeta_{gX}(\mathbf{q}') \rangle = \delta^{(3)}(\mathbf{q} + \mathbf{q}') \frac{2\pi^2}{q^3} \Delta_X^2(q) , \quad (2.3)$$

where \mathbf{q} denotes the wavevector, and a subscript X stands for S and L , respectively. For simplicity, we adopt a scale-invariant spectrum for Δ_L^2 , i.e., [113]

$$\Delta_L^2 = A_L \simeq 2.1 \times 10^{-9} . \quad (2.4)$$

We further assume Δ_S^2 to be a normal function with respect to $\ln q$, expressed as

$$\Delta_S^2(q) = \frac{A_S}{\sqrt{2\pi\sigma^2}} \exp \left[-\frac{\ln^2(q/q_*)}{2\sigma^2} \right] , \quad (2.5)$$

where σ represents the spectral width, q is the wavenumber, and A_S denotes the spectral amplitude at the peak wavenumber q_* . We consider a range of A_S spanning from 10^{-4} to 10^{-1} , which is particularly relevant in the context of PBH formation scenarios (see reviews in Refs. [93–95] and references therein). In the following, we set $\sigma = 1$ for the sake of simplicity, but other values can be readily accommodated if necessary. It is worth noting that the perturbativity imposes constraints on the model parameters, specifically $1 > 3|f_{\text{NL}}|\sqrt{A_S}/5 + 9|g_{\text{NL}}|A_S/25$ and $3|f_{\text{NL}}|\sqrt{A_S}/5 > 9|g_{\text{NL}}|A_S/25$.

The SIGWs can be divided into a homogeneous and isotropic background and the fluctuations on it, which are inhomogeneous and anisotropic. The former is described by the energy-density fraction spectrum $\bar{\Omega}_{\text{gw}}$, while the latter is described by the density contrast δ_{gw} , for which the statistical information is given by their correlation functions, such as the angular power spectrum, bispectrum, trispectrum, and so on. The contribution from ζ_{gL} to $\bar{\Omega}_{\text{gw}}$ is negligible due to $A_L \ll A_S$. In contrast, δ_{gw} is relevant with ζ_{gL} (or A_L equivalently) as the fluctuations arise from the couplings between ζ_{gL} and ζ_{gS} . We briefly review $\bar{\Omega}_{\text{gw}}$ in the following paragraph and leave the study of δ_{gw} to the subsequent sections.

The energy-density fraction spectrum $\bar{\Omega}_{\text{gw}}$ of SIGWs is defined by $\bar{\rho}_{\text{gw}}(\eta) = \rho_c(\eta) \int \bar{\Omega}_{\text{gw}}(\eta, q) d \ln q$ [114], where $\rho_c = 3\mathcal{H}^2/(8\pi G)$ represents the critical energy density of the universe at the conformal time η , \mathcal{H} denotes the conformal Hubble parameter, and the overbar signifies physical quantities at the background level. As a result, it is also associated with the four-point correlator of ζ , namely $\bar{\Omega}_{\text{gw}} \sim \langle \zeta^4 \rangle$. Based on Eqs. (2.1, 2.2, 2.5), we decompose it into nine components of the form [25]

$$\bar{\Omega}_{\text{gw}}^{(a,b)}(\eta_{\text{in}}, q) \propto \left(\frac{3}{5}f_{\text{NL}}\right)^{2a} \left(\frac{9}{25}g_{\text{NL}}\right)^b A_S^{a+b+2}, \quad (2.6)$$

where a and b are natural numbers satisfying the constraint $2a + b \leq 4$. They have been explicitly calculated via following the diagrammatic approach, which has been extensively employed in the literature [53–55, 71]. To be specific, they correspond to the diagrams illustrated in Table 2 and Figure 3 of Ref. [25], with the numerical results displayed in Figure 5 of Ref. [25]. In particular, $\bar{\Omega}_{\text{gw}}^{(0,0)}$ denotes the energy-density fraction spectrum of GWs produced by the Gaussian scalar perturbations, as demonstrated by the semi-analytic calculation in Refs. [20, 21]. In summary, we get

$$\bar{\Omega}_{\text{gw}} = \bar{\Omega}_{\text{gw}}^{(0,0)} + \bar{\Omega}_{\text{gw}}^{(0,1)} + \bar{\Omega}_{\text{gw}}^{(1,0)} + \bar{\Omega}_{\text{gw}}^{(0,2)} + \bar{\Omega}_{\text{gw}}^{(1,1)} + \bar{\Omega}_{\text{gw}}^{(2,0)} + \bar{\Omega}_{\text{gw}}^{(0,3)} + \bar{\Omega}_{\text{gw}}^{(1,2)} + \bar{\Omega}_{\text{gw}}^{(0,4)}. \quad (2.7)$$

As mentioned above, the contributions from both f_{NL} and g_{NL} to $\bar{\Omega}_{\text{gw}}(\eta_{\text{in}}, q)$ have been comprehensively analyzed in our existing work [25], with other studies available in Refs. [51–67, 71, 72].

For a given frequency band $\nu = q/(2\pi)$, the present-day energy-density fraction spectrum $\bar{\Omega}_{\text{gw},0}(\nu)$ is proportional to the energy-density fraction spectrum $\bar{\Omega}_{\text{gw}}$ introduced in Eq. (2.7). It is given by [115]

$$\bar{\Omega}_{\text{gw},0}(\nu) \simeq \Omega_{\text{r},0} \bar{\Omega}_{\text{gw}}(\eta_{\text{in}}, q), \quad (2.8)$$

where $\Omega_{\text{r},0} = 9.265 \times 10^{-5}$ is the present-day energy-density fraction of radiation in the universe [113]. In the above equation, we have neglected effects of the effective number of

relativistic degrees of freedom on the cosmic scale factor. They would not change our main results of this work, but lead to corrections of a factor of at most 2, which can be recovered if needed.

3 Angular correlation functions

We introduce the density contrast to quantify deviations from the homogeneous and isotropic background, given by [103, 104]

$$\delta_{\text{gw}}(\eta, \mathbf{x}, \mathbf{q}) = 4\pi \frac{\omega_{\text{gw}}(\eta, \mathbf{x}, \mathbf{q})}{\bar{\Omega}_{\text{gw}}(\eta, q)} - 1, \quad (3.1)$$

where the energy-density full spectrum ω_{gw} is defined by $\rho_{\text{gw}}(\eta, \mathbf{x}) = \rho_c(\eta) \int d \ln q d^2 \hat{\mathbf{q}} \omega_{\text{gw}}(\eta, \mathbf{x}, \mathbf{q})$. Furthermore, the energy density of SIGWs is explicitly expressed as $\rho_{\text{gw}} = \overline{\partial_l h_{ij} \partial_l h_{ij}} / (128\pi G a^2)$, where $a(\eta)$ is the scale factor of the universe, the long overbar stands for an oscillation average, and the semi-analytic formula of the SIGW strain $h_{ij}(\eta, \mathbf{q})$ is available in Refs. [20, 21]. Therefore, we have

$$\omega_{\text{gw}}(\eta, \mathbf{x}, \mathbf{q}) = -\frac{q^3}{48\mathcal{H}^2} \int \frac{d^3 \mathbf{k}}{(2\pi)^3} e^{i\mathbf{k}\cdot\mathbf{x}} [(\mathbf{k} - \mathbf{q}) \cdot \mathbf{q}] \overline{h_{ij}(\eta, \mathbf{k} - \mathbf{q}) h_{ij}(\eta, \mathbf{q})}, \quad (3.2)$$

which depends on both q and the direction $\hat{\mathbf{q}}$. Averaging over a vast number of Hubble horizons around \mathbf{x} at the production time yields $\langle \omega_{\text{gw}}(\eta, \mathbf{x}, \mathbf{q}) \rangle_{\mathbf{x}} = \bar{\Omega}_{\text{gw}}(\eta, q) / (4\pi)$, confirming the condition $\langle \delta_{\text{gw}}(\eta, \mathbf{x}, \mathbf{q}) \rangle_{\mathbf{x}} = 0$.

Based on the Boltzmann equation [103, 104, 116], the present-day density contrast $\delta_{\text{gw},0}(\mathbf{q}) = \delta_{\text{gw}}(\eta_0, \mathbf{x}_0, \mathbf{q})$ incorporates the initial inhomogeneity $\delta_{\text{gw}}(\eta_{\text{in}}, \mathbf{x}, \mathbf{q})$ and the propagation effects. It is given by [25, 70–72]

$$\delta_{\text{gw},0}(\mathbf{q}) = \delta_{\text{gw}}(\eta_{\text{in}}, \mathbf{x}, \mathbf{q}) + [4 - n_{\text{gw}}(\nu)] \Phi(\eta_{\text{in}}, \mathbf{x}), \quad (3.3)$$

where the metric scalar perturbation $\Phi(\eta_{\text{in}}, \mathbf{x})$ represents the Sachs-Wolfe (SW) effect [117], and the energy-density fraction spectral index, defined as

$$n_{\text{gw}}(\nu) = \frac{\partial \ln \bar{\Omega}_{\text{gw},0}(\nu)}{\partial \ln \nu}, \quad (3.4)$$

is approximated to be time-independent owing to Eq. (2.8). Here, we disregard the integrated Sachs-Wolfe (ISW) effect and the gravitational lensing effect. The ISW effect is relatively less significant than the SW effect [70], while the gravitational lensing effect is of higher order compared with the SW effect [103, 104] and is expected to primarily impact $\delta_{\text{gw},0}$ at higher multipoles [15]. Nevertheless, it is straightforward to extend our analysis to include all of them.

The angular correlators encode statistical information of the inhomogeneity and anisotropy of SIGWs. We introduce $\delta_{\text{gw},0,\ell m}(2\pi\nu)$ to represent the decomposition of $\delta_{\text{gw},0}(\mathbf{q})$ in terms of spherical harmonics, as given by

$$\delta_{\text{gw},0}(\mathbf{q}) = \sum_{\ell m} \delta_{\text{gw},0,\ell m}(q) Y_{\ell m}(\hat{\mathbf{q}}). \quad (3.5)$$

The two-point correlator gives rise to the reduced angular power spectrum, i.e.,

$$\left\langle \delta_{\text{gw},0,\ell m}(2\pi\nu) \delta_{\text{gw},0,\ell' m'}^*(2\pi\nu) \right\rangle = \delta_{\ell\ell'} \delta_{mm'} \tilde{C}_\ell(\nu), \quad (3.6)$$

which has been extensively investigated in Refs. [25, 70, 71, 94, 118–127]. In this work, we introduce the (reduced) angular bispectrum and trispectrum to capture the non-Gaussianity of GW background, analogue to CMB.

The angular bispectrum for the rotation-invariant GW background is factorized through the three-point correlator, i.e.,

$$\left\langle \prod_{i=1}^3 \delta_{\text{gw},0,\ell_i m_i}(2\pi\nu) \right\rangle = \mathcal{G}_{\ell_1 \ell_2 \ell_3}^{m_1 m_2 m_3} \tilde{b}_{\ell_1 \ell_2 \ell_3}(\nu), \quad (3.7)$$

where the Gaunt integral $\mathcal{G}_{\ell_1 \ell_2 \ell_3}^{m_1 m_2 m_3}$ arises from the assumption of statistical isotropy and parity invariance, as expressed in terms of the Wigner 3- j symbols, i.e.,

$$\mathcal{G}_{\ell_1 \ell_2 \ell_3}^{m_1 m_2 m_3} = h_{\ell_1 \ell_2 \ell_3} \begin{pmatrix} \ell_1 & \ell_2 & \ell_3 \\ m_1 & m_2 & m_3 \end{pmatrix}, \quad (3.8)$$

where we define

$$h_{\ell_1 \ell_2 \ell_3} = \sqrt{\frac{(2\ell_1 + 1)(2\ell_2 + 1)(2\ell_3 + 1)}{4\pi}} \begin{pmatrix} \ell_1 & \ell_2 & \ell_3 \\ 0 & 0 & 0 \end{pmatrix}. \quad (3.9)$$

Moreover, we recall that the tetrahedral domain of multipole triplets $\{\ell_1, \ell_2, \ell_3\}$ satisfies both the triangular inequalities ($\ell_1 \leq \ell_2 + \ell_3$, $\ell_2 \leq \ell_1 + \ell_3$, $\ell_3 \leq \ell_1 + \ell_2$, and $m_1 + m_2 + m_3 = 0$) and the parity condition ($\ell_1 + \ell_2 + \ell_3 = 2n$, $n \in \mathbb{N}$), which are identical to those in the study of CMB [128, 129].

Going to higher-order statistic, the four-point correlator defines the angular trispectrum. Analogous to that of CMB [130–132], the angular trispectrum of a rotationally invariant GW background takes the following form

$$\left\langle \prod_{i=1}^4 \delta_{\text{gw},0,\ell_i m_i}(2\pi\nu) \right\rangle = \sum_{LM} (-1)^M \begin{pmatrix} \ell_1 & \ell_2 & L \\ m_1 & m_2 & -M \end{pmatrix} \begin{pmatrix} \ell_3 & \ell_4 & L \\ m_3 & m_4 & M \end{pmatrix} T_{\ell_3 \ell_4}^{\ell_1 \ell_2}(L, \nu). \quad (3.10)$$

where $T_{\ell_3 \ell_4}^{\ell_1 \ell_2}(L, \nu)$ stands for the angular averaged trispectrum. The Wigner 3- j symbols imply that the quadrilateral $\{\ell_1, \ell_2, \ell_3, \ell_4\}$ is divided into two triangles ($\{\ell_1, \ell_2, L\}$ and $\{\ell_3, \ell_4, L\}$) by a diagonal, which results in the triangular conditions $|\ell_1 - \ell_2| < L < \ell_1 + \ell_2$ and $|\ell_3 - \ell_4| < L < \ell_3 + \ell_4$ and $m_1 + m_2 - M = m_3 + m_4 + M = 0$. Moreover, $\ell_1 + \ell_2 + \ell_3 + \ell_4$ are required to be even as the result of parity invariance. Further, $T_{\ell_3 \ell_4}^{\ell_1 \ell_2}(L, \nu)$ can be decomposed into the disconnected part, denoted as $T_{G_{\ell_3 \ell_4}}^{\ell_1 \ell_2}(L, \nu)$, and the connected part, denoted as $T_{c_{\ell_3 \ell_4}}^{\ell_1 \ell_2}(L, \nu)$, i.e.,

$$T_{\ell_3 \ell_4}^{\ell_1 \ell_2}(L, \nu) = T_{G_{\ell_3 \ell_4}}^{\ell_1 \ell_2}(L, \nu) + T_{c_{\ell_3 \ell_4}}^{\ell_1 \ell_2}(L, \nu). \quad (3.11)$$

The former corresponds to the Gaussian case, and thus can be expressed in terms of $\tilde{C}_\ell(\nu)$, namely,

$$\begin{aligned} T_{G_{\ell_3 \ell_4}}^{\ell_1 \ell_2}(L, \nu) &= (-1)^{\ell_1 + \ell_3} \sqrt{(2\ell_1 + 1)(2\ell_3 + 1)} \tilde{C}_{\ell_1}(\nu) \tilde{C}_{\ell_3}(\nu) \delta_{\ell_1 \ell_2} \delta_{\ell_3 \ell_4} \delta_{L0} \\ &\quad + (2L + 1) \tilde{C}_{\ell_1}(\nu) \tilde{C}_{\ell_2}(\nu) \left[(-1)^{\ell_1 + \ell_2 + L} \delta_{\ell_1 \ell_3} \delta_{\ell_2 \ell_4} + \delta_{\ell_1 \ell_4} \delta_{\ell_2 \ell_3} \right]. \end{aligned} \quad (3.12)$$

In contrast, the later features the non-Gaussianity of SIGW background. By using the Wigner 6- j symbol to account for the permutation symmetry, we can explicitly express it in the form of

$$T_{c_{\ell_3 \ell_4}}^{\ell_1 \ell_2}(L, \nu) = P_{\ell_3 \ell_4}^{\ell_1 \ell_2}(L, \nu) + (2L + 1) \sum_{L'} \left[(-1)^{\ell_2 + \ell_3} \begin{Bmatrix} \ell_1 & \ell_2 & L' \\ \ell_4 & \ell_3 & L \end{Bmatrix} P_{\ell_2 \ell_4}^{\ell_1 \ell_3}(L', \nu) \right. \\ \left. + (-1)^{L+L'} \begin{Bmatrix} \ell_1 & \ell_2 & L' \\ \ell_3 & \ell_4 & L \end{Bmatrix} P_{\ell_3 \ell_2}^{\ell_1 \ell_4}(L', \nu) \right], \quad (3.13)$$

where $P_{\ell_3 \ell_4}^{\ell_1 \ell_2}(L, \nu)$ is written in terms of the reduced angular trispectrum $t_{\ell_3 \ell_4}^{\ell_1 \ell_2}(L, \nu)$, namely,

$$P_{\ell_3 \ell_4}^{\ell_1 \ell_2}(L, \nu) = t_{\ell_3 \ell_4}^{\ell_1 \ell_2}(L, \nu) + (-1)^{\ell_1 + \ell_2 + L} t_{\ell_3 \ell_4}^{\ell_2 \ell_1}(L, \nu) + (-1)^{\ell_3 + \ell_4 + L} t_{\ell_4 \ell_3}^{\ell_1 \ell_2}(L, \nu) + (-1)^{\ell_1 + \ell_2 + \ell_3 + \ell_4 + 2L} t_{\ell_4 \ell_3}^{\ell_2 \ell_1}(L, \nu). \quad (3.14)$$

Notably, due to the parity invariance, the reduced angular trispectrum obeys $t_{\ell_3 \ell_4}^{\ell_1 \ell_2}(L, \nu) = t_{\ell_4 \ell_3}^{\ell_2 \ell_1}(L, \nu)$. Moreover, the permutation symmetry requires that it is symmetric against exchange of its upper and lower indices, namely, $t_{\ell_3 \ell_4}^{\ell_1 \ell_2}(L, \nu) = t_{\ell_1 \ell_2}^{\ell_3 \ell_4}(L, \nu)$. Obviously, the disconnected part $T_G^{\ell_1 \ell_2}(L, \nu)$ vanishes if all the four multipoles are not equal, so that the angular averaged trispectrum is just the connected part $T_{c_{\ell_3 \ell_4}}^{\ell_1 \ell_2}(L, \nu)$. Due to limitations in the angular resolutions of ongoing and planned GW detectors [37, 120, 133–139], we consider only the low multipoles ℓ in our present work. However, it is straightforward to generalize our analysis to higher multipoles ℓ if needed.

4 Semi-analytic formulae for angular bispectrum and trispectrum

We employ the diagrammatic approach [25, 71] to derive the semi-analytic formulae for the angular bispectrum and trispectrum of SIGWs. As defined in Eq. (3.7), $\tilde{b}_{\ell_1 \ell_2 \ell_3}$ and $t_{\ell_3 \ell_4}^{\ell_1 \ell_2}(L, \nu)$ are related with the three- and four-point correlators of $\delta_{\text{gw},0}(\mathbf{q})$, respectively, which is introduced by Eq. (3.3). While the correlations involving the SW effect alone can be straightforwardly evaluated, our calculation of the correlations involving the initial inhomogeneities $\delta_{\text{gw}}(\eta_{\text{in}}, \mathbf{x}, \mathbf{q})$ would result in multi-point correlations of the form $\langle \omega_{\text{gw}}^3 \rangle \sim \langle h^6 \rangle \sim \langle \zeta^{12} \rangle$ for $\tilde{b}_{\ell_1 \ell_2 \ell_3}$ and $\langle \omega_{\text{gw}}^4 \rangle \sim \langle h^8 \rangle \sim \langle \zeta^{16} \rangle$ for $t_{\ell_3 \ell_4}^{\ell_1 \ell_2}(L, \nu)$. When Eq. (2.1) is further considered, it is particularly challenging to evaluate these correlations, since they involve correlations of the order at most $\langle \zeta_g^{36} \rangle$ and $\langle \zeta_g^{48} \rangle$, respectively. As demonstrated by Ref. [25], however, the diagrammatic approach transforms the multi-point correlators of non-Gaussian ζ into combinations of connections among different ζ vertices, thus significantly simplifying our calculations. Based on Eq. (2.1), the relationship between the primordial non-Gaussian curvature perturbations ζ up to g_{NL} order and their Gaussian components ζ_g can be represented via three types of vertices, as shown in Figure 1 and named from left to right as the Gaussian-vertex, the f_{NL} -vertex, and the g_{NL} -vertex.

Following the Feynman-like rules in Ref. [25], we are able to depict the connected Feynman-like diagrams for the multi-point correlators of $\omega_{\text{gw}}(\eta_{\text{in}}, \mathbf{k}_i, \mathbf{q}_i)$, which is the Fourier mode of $\omega_{\text{gw}}(\eta_{\text{in}}, \mathbf{x}_i, \mathbf{q}_i)$. For the three-point correlator $\langle \prod_{i=1}^3 \omega_{\text{gw}}(\eta_{\text{in}}, \mathbf{k}_i, \mathbf{q}_i) \rangle$ at leading order of A_L , one typical Feynman-like diagram is demonstrated in the left panel of Figure 2. In the

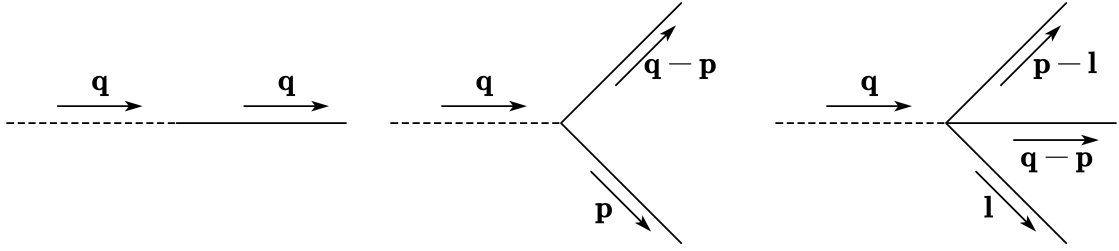


Figure 1: Gaussian-vertex, f_{NL} -vertex, and g_{NL} -vertex.

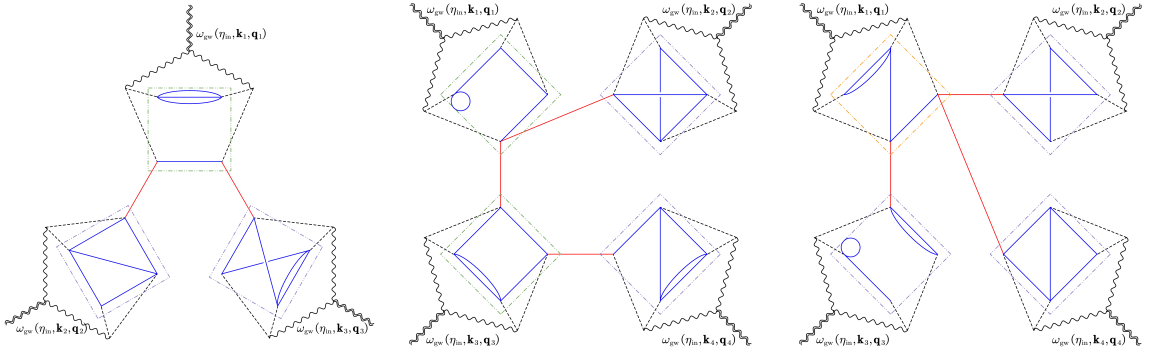


Figure 2: One of the Feynman-like diagrams for the three-point correlator of $\omega_{\text{gw}}(\eta_{\text{in}}, \mathbf{k}, \mathbf{q})$ (left) and two of the Feynman-like diagrams for the four-point correlator of $\omega_{\text{gw}}(\eta_{\text{in}}, \mathbf{k}, \mathbf{q})$ (middle and right). Other Feynman-like diagrams can be obtained via replacing the dotted-dashed boxes with certain panels of Figure 3 in Ref. [25], following an explicit approach demonstrated in the context. Here, double wavy lines denote the energy-density full spectrum ω_{gw} , single wavy lines denote the GW strain h , dashed lines denote the scalar transfer functions, and solid lines denote the primordial curvature power spectra for the Gaussian components ζ_g . Especially, the power spectrum of ζ_{gS} is represented as blue solid lines, while the power spectrum of ζ_{gL} are represented as red solid lines.

diagram, the initial inhomogeneities ω_{gw} situate at distinct positions, are connected by “non-Gaussian bridges” (denoted as red solid lines), which symbolize the power spectra of ζ_{gL} . These connections stand for the redistribution of the SIGW energy density on large scales. Given that $A_L \ll A_S$, diagrams with more than two “non-Gaussian bridges” contribute little to the bispectrum and are discarded. In addition, the difference between other Feynman-like diagrams and this one lies in the different ways that the blue or red solid lines connect the vertices within the three dashed boxes. Likewise, when considering the four-point correlator $\langle \prod_{i=1}^4 \omega_{\text{gw}}(\eta_{\text{in}}, \mathbf{k}_i, \mathbf{q}_i) \rangle$ at leading order of A_L , two typical Feynman-like diagrams on behalf of two types of connections via “non-Gaussian bridges” are depicted in the middle and right panels of Figure 2. We are able to obtain other Feynman-like diagrams with three “non-Gaussian bridges” through replacing the four dotted-dashed boxes, while the Feynman-like diagrams with more than three “non-Gaussian bridges” are discarded as they are negligible.

As demonstrated by our existing work [25], it is convenient to expand $\omega_{\text{gw}}(\eta_{\text{in}}, \mathbf{x}_i, \mathbf{q}_i)$

up to $\mathcal{O}(\zeta_{gL}^3)$ before calculating the correlations, which simplifies the replacement of the four dotted-dashed boxes and avoids computing the cross-correlation of the initial term and the propagation term. Using Eqs. (2.1,2.2,3.2) and $h_{ij} \sim \zeta^2$, we can express $\omega_{\text{gw}}(\eta_{\text{in}}, \mathbf{x}_i, \mathbf{q}_i)$ schematically through the Wick contractions as follows

$$\begin{aligned}
\omega_{\text{gw}}(\eta_{\text{in}}, \mathbf{x}_i, \mathbf{q}_i) &\sim \langle \zeta^4 \rangle_{\mathbf{x}_i} \\
&\sim \langle \zeta_S^4 \rangle_{\mathbf{x}_i} + \mathcal{O}(\zeta_{gL}) [f_{\text{NL}} \langle \zeta_{gS} \zeta_S^3 \rangle_{\mathbf{x}_i} + g_{\text{NL}} \langle \zeta_{gS}^2 \zeta_S^3 \rangle_{\mathbf{x}_i}] \\
&\quad + \mathcal{O}(\zeta_{gL}^2) [f_{\text{NL}}^2 \langle \zeta_{gS}^2 \zeta_S^2 \rangle_{\mathbf{x}_i} + f_{\text{NL}} g_{\text{NL}} \langle \zeta_{gS}^3 \zeta_S^2 \rangle_{\mathbf{x}_i} + g_{\text{NL}}^2 \langle \zeta_{gS}^4 \zeta_S^2 \rangle_{\mathbf{x}_i} + g_{\text{NL}} \langle \zeta_{gS} \zeta_S^3 \rangle_{\mathbf{x}_i}] \\
&\quad + \mathcal{O}(\zeta_{gL}^3) [f_{\text{NL}}^3 \langle \zeta_{gS}^3 \zeta_S \rangle_{\mathbf{x}_i} + f_{\text{NL}}^2 g_{\text{NL}} \langle \zeta_{gS}^4 \zeta_S \rangle_{\mathbf{x}_i} + f_{\text{NL}} g_{\text{NL}}^2 \langle \zeta_{gS}^5 \zeta_S \rangle_{\mathbf{x}_i} \\
&\quad\quad + g_{\text{NL}}^3 \langle \zeta_{gS}^6 \zeta_S \rangle_{\mathbf{x}_i} + f_{\text{NL}} g_{\text{NL}} \langle \zeta_{gS}^2 \zeta_S^2 \rangle_{\mathbf{x}_i} + g_{\text{NL}}^2 \langle \zeta_{gS}^3 \zeta_S^2 \rangle_{\mathbf{x}_i}] , \tag{4.1}
\end{aligned}$$

where ζ_S represents the short-wavelength modes including both the Gaussian and non-Gaussian components. Notably, the ensemble average within the observed region centered at \mathbf{x}_i is necessary, as the observed signal along a line-of-sight is a combination of SIGWs originating from numerous small-scale regions, owing to limitations in the angular resolution of GW detectors. Furthermore, the leading term $\langle \zeta_S^4 \rangle_{\mathbf{x}}$ corresponds to the background $\bar{\Omega}_{\text{gw}}/(4\pi)$ exactly, while others should be combinations of $\bar{\Omega}_{\text{gw}}^{(a,b)}$ that contribute to the energy-density fluctuations on large scales, as demonstrated in the following.

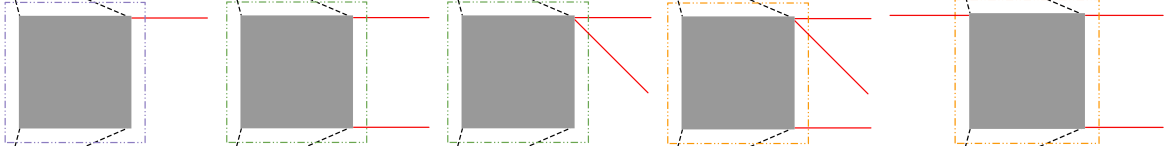


Figure 3: Dotted-dashed boxes in Figure 2 featuring $\omega_{\text{gw}}(\eta_{\text{in}}, \mathbf{x}_i, \mathbf{q}_i)$ at various orders in ζ_{gL} . The shadow squares should be replaced with one of the panels of Figure 3 in Ref. [25].

As indicated by Figure 3, the dotted-dashed boxes can be used for representations of $\omega_{\text{gw}}(\eta_{\text{in}}, \mathbf{x}_i, \mathbf{q}_i)$ at different orders in ζ_{gL} . From left to right, the first box represents $\omega_{\text{gw}}(\eta_{\text{in}}, \mathbf{x}_i, \mathbf{q}_i)$ at $\mathcal{O}(\zeta_{gL})$ order, the second and third boxes represent $\omega_{\text{gw}}(\eta_{\text{in}}, \mathbf{x}_i, \mathbf{q}_i)$ at $\mathcal{O}(\zeta_{gL}^2)$ order and the last two panels represents $\omega_{\text{gw}}(\eta_{\text{in}}, \mathbf{x}_i, \mathbf{q}_i)$ at $\mathcal{O}(\zeta_{gL}^3)$ order. The shadow squares cover the connections of blue solid lines which correspond to the correlators between ζ_{gS} and ζ_S in Eq. (4.1). They should be replaced with specific panels of Figure 3 in Ref. [25], based on the count of Gaussian-vertices, f_{NL} -vertices, and g_{NL} -vertices in each panel. To be specific, for $\bar{\Omega}_{\text{gw}}^{(a,b)}$, we can straightforwardly express the count of f_{NL} -vertices as $N_{f_{\text{NL}}}^{(a,b)} = 2a$ and the count of g_{NL} -vertices as $N_{g_{\text{NL}}}^{(a,b)} = b$. As $\bar{\Omega}_{\text{gw}} \sim \langle \zeta^4 \rangle$ indicates that four vertices are involved in the propagators of ζ in total, the count of Gaussian-vertices is $N_{\text{Gau}}^{(a,b)} = 4 - 2a - b$. We will provide a detailed explanation of the conditions that the panels replacing these shadow squares need to satisfy in the following.

In fact, a simple approach to obtain the explicit expression of Eq. (4.1) is to identify all allowable connections among the three (four) $\omega_{\text{gw}}(\eta_{\text{in}}, \mathbf{k}_i, \mathbf{q}_i)$ via three (four) “non-Gaussian bridges”. Compared with the vertices before connection, the inclusion of the “non-Gaussian bridges” results in the transformation of a vertex into another vertex that represents non-

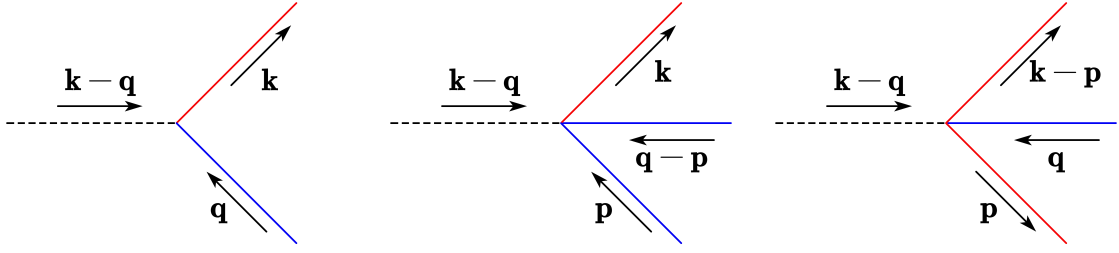


Figure 4: Vertices involved in the non-Gaussian bridges.

Gaussian parameters of higher order, as illustrated in Figure 4. For contractions at $\mathcal{O}(\zeta_{gL})$ order that correspond to the first panel of Figure 3, there are two allowable transformations:

- As depicted in the left panel of Figure 4, one Gaussian-vertex is transformed into an f_{NL} -vertex, which also doubles the symmetric factor.
- As depicted in the middle panel of Figure 4, one f_{NL} -vertex is transformed into a g_{NL} -vertex, which triples the symmetric factor.

Similarly, for contractions at $\mathcal{O}(\zeta_{gL}^2)$ order that correspond to the second and third panels of Figure 3, there are four allowable transformations:

- Two Gaussian-vertices are transformed into f_{NL} -vertices, respectively.
- Two f_{NL} -vertices are transformed into g_{NL} -vertices, respectively.
- One Gaussian-vertex is transformed into an f_{NL} -vertex and one f_{NL} -vertex is transformed into a g_{NL} -vertex.
- As depicted in the right panel of Figure 4, one Gaussian-vertex is transformed into a g_{NL} -vertex, which sextuples the symmetric factor.

For contractions at $\mathcal{O}(\zeta_{gL}^3)$ order that correspond to the last two panels of Figure 3, there are six allowable transformations:

- Three Gaussian-vertices are transformed into f_{NL} -vertices, respectively.
- Three f_{NL} -vertices are transformed into g_{NL} -vertices, respectively.
- Two Gaussian-vertices are transformed into f_{NL} -vertices and one f_{NL} -vertex is transformed into a g_{NL} -vertex.
- One Gaussian-vertex is transformed into an f_{NL} -vertex and two f_{NL} -vertices are transformed into a g_{NL} -vertices.
- One Gaussian-vertex is transformed into an f_{NL} -vertex and another Gaussian-vertex is transformed into a g_{NL} -vertex.
- One Gaussian-vertex is transformed into a g_{NL} -vertex and one f_{NL} -vertex is transformed into a g_{NL} -vertex.

Accordingly, only the panels of Figure 3 in Ref. [25] that contain a sufficient count of Gaussian-vertices and f_{NL} -vertices can replace the shadow squares in the corresponding boxes.

In summary, when considering the correlation functions of $\omega_{\text{gw}}(\eta_{\text{in}}, \mathbf{x}, \mathbf{q})$, the initial energy-density full spectrum in Eq. (4.1) can be expressed in the form of

$$\begin{aligned} \omega_{\text{gw}}(\eta_{\text{in}}, \mathbf{x}, \mathbf{q}) &= \frac{\bar{\Omega}_{\text{gw}}(\eta_{\text{in}}, q)}{4\pi} + \frac{\Omega_{\text{ng}}^{(1)}(\eta_{\text{in}}, q)}{4\pi} \int \frac{d^3\mathbf{k}}{(2\pi)^{3/2}} e^{i\mathbf{k}\cdot\mathbf{x}} \zeta_{gL}(\mathbf{k}) \\ &+ \frac{\Omega_{\text{ng}}^{(2)}(\eta_{\text{in}}, q)}{4\pi} \int \frac{d^3\mathbf{k} d^3\mathbf{p}}{(2\pi)^3} e^{i\mathbf{k}\cdot\mathbf{x}} \zeta_{gL}(\mathbf{p}) \zeta_{gL}(\mathbf{k} - \mathbf{p}) \\ &+ \frac{\Omega_{\text{ng}}^{(3)}(\eta_{\text{in}}, q)}{4\pi} \int \frac{d^3\mathbf{k} d^3\mathbf{p} d^3\mathbf{l}}{(2\pi)^{9/2}} e^{i\mathbf{k}\cdot\mathbf{x}} \zeta_{gL}(\mathbf{l}) \zeta_{gL}(\mathbf{p} - \mathbf{l}) \zeta_{gL}(\mathbf{k} - \mathbf{p}) , \end{aligned} \quad (4.2)$$

where $\Omega_{\text{ng}}^{(1)}(\eta_{\text{in}}, q)$, corresponding to the first panel of Figure 3, is identical to that in our existing work [25], i.e.,

$$\begin{aligned} \Omega_{\text{ng}}^{(1)}(\eta_{\text{in}}, q) &= \sum_{(a,b)} \left[\left(2 \times \frac{3f_{\text{NL}}/5}{1} \right) \binom{N_{\text{Gau}}^{(a,b)}}{1} + \left(3 \times \frac{9g_{\text{NL}}/25}{3f_{\text{NL}}/5} \right) \binom{N_{f_{\text{NL}}}^{(a,b)}}{1} \right] \bar{\Omega}_{\text{gw}}^{(a,b)} \\ &= \frac{6f_{\text{NL}}}{5} \left(4\bar{\Omega}_{\text{gw}}^{(0,0)} + 3\bar{\Omega}_{\text{gw}}^{(0,1)} + 2\bar{\Omega}_{\text{gw}}^{(1,0)} + 2\bar{\Omega}_{\text{gw}}^{(0,2)} + \bar{\Omega}_{\text{gw}}^{(1,1)} + \bar{\Omega}_{\text{gw}}^{(0,3)} \right) \\ &+ \frac{9g_{\text{NL}}}{5f_{\text{NL}}} \left(2\bar{\Omega}_{\text{gw}}^{(1,0)} + 2\bar{\Omega}_{\text{gw}}^{(1,1)} + 4\bar{\Omega}_{\text{gw}}^{(2,0)} + 2\bar{\Omega}_{\text{gw}}^{(1,2)} \right) , \end{aligned} \quad (4.3)$$

$\Omega_{\text{ng}}^{(2)}(\eta_{\text{in}}, q)$, corresponding to the second and third panels of Figure 3, is derived for the first time, given by

$$\begin{aligned} \Omega_{\text{ng}}^{(2)}(\eta_{\text{in}}, q) &= \sum_{(a,b)} \left[\left(2 \times \frac{3f_{\text{NL}}/5}{1} \right)^2 \binom{N_{\text{Gau}}^{(a,b)}}{2} + \left(3 \times \frac{9g_{\text{NL}}/25}{3f_{\text{NL}}/5} \right)^2 \binom{N_{f_{\text{NL}}}^{(a,b)}}{2} \right. \\ &+ \left(2 \times \frac{3f_{\text{NL}}/5}{1} \right) \left(3 \times \frac{9g_{\text{NL}}/25}{3f_{\text{NL}}/5} \right) \binom{N_{\text{Gau}}^{(a,b)}}{1} \binom{N_{f_{\text{NL}}}^{(a,b)}}{1} \\ &+ \left. \left(6 \times \frac{9g_{\text{NL}}/25}{1} \right) \binom{N_{\text{Gau}}^{(a,b)}}{1} \right] \bar{\Omega}_{\text{gw}}^{(a,b)} \\ &= \left(\frac{6f_{\text{NL}}}{5} \right)^2 \left(6\bar{\Omega}_{\text{gw}}^{(0,0)} + 3\bar{\Omega}_{\text{gw}}^{(0,1)} + \bar{\Omega}_{\text{gw}}^{(1,0)} + \bar{\Omega}_{\text{gw}}^{(0,2)} \right) \\ &+ \left(\frac{9g_{\text{NL}}}{5f_{\text{NL}}} \right)^2 \left(\bar{\Omega}_{\text{gw}}^{(1,0)} + \bar{\Omega}_{\text{gw}}^{(1,1)} + 6\bar{\Omega}_{\text{gw}}^{(2,0)} + \bar{\Omega}_{\text{gw}}^{(1,2)} \right) \\ &+ \frac{54g_{\text{NL}}}{25} \left(4\bar{\Omega}_{\text{gw}}^{(0,0)} + 3\bar{\Omega}_{\text{gw}}^{(0,1)} + 6\bar{\Omega}_{\text{gw}}^{(1,0)} + 2\bar{\Omega}_{\text{gw}}^{(0,2)} + 3\bar{\Omega}_{\text{gw}}^{(1,1)} + \bar{\Omega}_{\text{gw}}^{(0,3)} \right) . \end{aligned} \quad (4.4)$$

and $\Omega_{\text{ng}}^{(3)}(\eta_{\text{in}}, q)$, corresponding to the last two panels of Figure 3, is also derived for the first

time, given by

$$\begin{aligned}
\Omega_{\text{ng}}^{(3)}(\eta_{\text{in}}, q) &= \sum_{(a,b)} \left[\left(2 \times \frac{3f_{\text{NL}}/5}{1} \right)^3 \binom{N_{\text{Gau}}^{(a,b)}}{3} + \left(3 \times \frac{9g_{\text{NL}}/25}{3f_{\text{NL}}/5} \right)^3 \binom{N_{f_{\text{NL}}}^{(a,b)}}{3} \right. \\
&\quad + \left(2 \times \frac{3f_{\text{NL}}/5}{1} \right)^2 \left(3 \times \frac{9g_{\text{NL}}/25}{3f_{\text{NL}}/5} \right) \binom{N_{\text{Gau}}^{(a,b)}}{2} \binom{N_{f_{\text{NL}}}^{(a,b)}}{1} \\
&\quad + \left(2 \times \frac{3f_{\text{NL}}/5}{1} \right) \left(3 \times \frac{9g_{\text{NL}}/25}{3f_{\text{NL}}/5} \right)^2 \binom{N_{\text{Gau}}^{(a,b)}}{1} \binom{N_{f_{\text{NL}}}^{(a,b)}}{2} \\
&\quad + \left(6 \times \frac{9g_{\text{NL}}/25}{1} \right) \left(2 \times \frac{3f_{\text{NL}}/5}{1} \right) N_{\text{Gau}}^{(a,b)} (N_{\text{Gau}}^{(a,b)} - 1) \\
&\quad \left. + \left(6 \times \frac{9g_{\text{NL}}/25}{1} \right) \left(3 \times \frac{9g_{\text{NL}}/25}{3f_{\text{NL}}/5} \right) \binom{N_{\text{Gau}}^{(a,b)}}{1} \binom{N_{f_{\text{NL}}}^{(a,b)}}{1} \right] \bar{\Omega}_{\text{gw}}^{(a,b)} \\
&= \left(\frac{6f_{\text{NL}}}{5} \right)^3 \left(4\bar{\Omega}_{\text{gw}}^{(0,0)} + \bar{\Omega}_{\text{gw}}^{(0,1)} \right) \\
&\quad + 3 \times \left(\frac{6}{5} \right)^3 f_{\text{NL}} g_{\text{NL}} \left(6\bar{\Omega}_{\text{gw}}^{(0,0)} + 3\bar{\Omega}_{\text{gw}}^{(0,1)} + 2\bar{\Omega}_{\text{gw}}^{(1,0)} + \bar{\Omega}_{\text{gw}}^{(0,2)} \right) \\
&\quad + 2 \times \left(\frac{9}{5} \right)^3 \frac{g_{\text{NL}}^2}{f_{\text{NL}}} \left(2\bar{\Omega}_{\text{gw}}^{(1,0)} + \bar{\Omega}_{\text{gw}}^{(1,1)} \right) + 4 \times \left(\frac{9g_{\text{NL}}}{5f_{\text{NL}}} \right)^3 \bar{\Omega}_{\text{gw}}^{(2,0)}. \tag{4.5}
\end{aligned}$$

Notably, despite the presence of f_{NL} in denominators in Eqs. (4.3,4.4,4.5), the value of f_{NL} could be taken as zero, since $\bar{\Omega}_{\text{gw}}^{(a,b)}$ is proportional to f_{NL}^{2a} and thus f_{NL} disappears from the denominators after reduction. It is further observed that $\Omega_{\text{ng}}^{(3)}$ becomes zero when $f_{\text{NL}} = 0$.

Therefore, the present-day density contrast of SIGWs, as defined in Eq. (3.3), can be decomposed into three terms according to their orders in ζ_{gL} , namely

$$\delta_{\text{gw},0}(\mathbf{q}) = \delta_{\text{gw},0}^{(1)}(\mathbf{q}) + \delta_{\text{gw},0}^{(2)}(\mathbf{q}) + \delta_{\text{gw},0}^{(3)}(\mathbf{q}), \tag{4.6}$$

where we introduce three quantities of the form

$$\delta_{\text{gw},0}^{(1)}(\mathbf{q}) = \left\{ \frac{\Omega_{\text{ng}}^{(1)}(\eta_{\text{in}}, 2\pi\nu)}{\bar{\Omega}_{\text{gw}}(\eta_{\text{in}}, 2\pi\nu)} + \frac{3}{5} [4 - n_{\text{gw}}(\nu)] \right\} \int \frac{d^3\mathbf{k}}{(2\pi)^{3/2}} e^{i\mathbf{k}\cdot\mathbf{x}} \zeta_{gL}(\mathbf{k}), \tag{4.7}$$

$$\delta_{\text{gw},0}^{(2)}(\mathbf{q}) = \left\{ \frac{\Omega_{\text{ng}}^{(2)}(\eta_{\text{in}}, 2\pi\nu)}{\bar{\Omega}_{\text{gw}}(\eta_{\text{in}}, 2\pi\nu)} + \frac{9}{25} f_{\text{NL}} [4 - n_{\text{gw}}(\nu)] \right\} \int \frac{d^3\mathbf{k} d^3\mathbf{p}}{(2\pi)^3} e^{i\mathbf{k}\cdot\mathbf{x}} \zeta_{gL}(\mathbf{p}) \zeta_{gL}(\mathbf{k} - \mathbf{p}), \tag{4.8}$$

$$\delta_{\text{gw},0}^{(3)}(\mathbf{q}) = \left\{ \frac{\Omega_{\text{ng}}^{(3)}(\eta_{\text{in}}, 2\pi\nu)}{\bar{\Omega}_{\text{gw}}(\eta_{\text{in}}, 2\pi\nu)} + \frac{27}{125} g_{\text{NL}} [4 - n_{\text{gw}}(\nu)] \right\} \int \frac{d^3\mathbf{k} d^3\mathbf{p} d^3\mathbf{l}}{(2\pi)^{9/2}} e^{i\mathbf{k}\cdot\mathbf{x}} \zeta_{gL}(\mathbf{l}) \zeta_{gL}(\mathbf{p} - \mathbf{l}) \zeta_{gL}(\mathbf{k} - \mathbf{p}). \tag{4.9}$$

Here, as the long-wavelength mode reentered the Hubble horizon during matter domination, we have also considered the Bardeen potential up to third order in ζ_{gL} . It is now given by

$$\begin{aligned}
\Phi(\eta_{\text{in}}, \mathbf{x}) &= \frac{3}{5} \int \frac{d^3\mathbf{k}}{(2\pi)^{3/2}} e^{i\mathbf{k}\cdot\mathbf{x}} \left[\zeta_{gL}(\mathbf{k}) + \frac{3}{5} f_{\text{NL}} \int \frac{d^3\mathbf{p}}{(2\pi)^{3/2}} \zeta_{gL}(\mathbf{p}) \zeta_{gL}(\mathbf{k} - \mathbf{p}) \right. \\
&\quad \left. + \frac{9}{25} g_{\text{NL}} \int \frac{d^3\mathbf{p} d^3\mathbf{l}}{(2\pi)^3} e^{i\mathbf{k}\cdot\mathbf{x}} \zeta_{gL}(\mathbf{l}) \zeta_{gL}(\mathbf{p} - \mathbf{l}) \zeta_{gL}(\mathbf{k} - \mathbf{p}) \right]. \tag{4.10}
\end{aligned}$$

4.1 Angular bispectrum

For $\tilde{b}_{\ell_1\ell_2\ell_3}(\nu)$ in Eq. (3.7), an integral is involved due to the three-point correlation function of $\delta_{\text{gw},0}$ in ℓ, m space. Non-vanishing contractions at leading order in A_L comprise two $\delta_{\text{gw},0}^{(1)}$ and one $\delta_{\text{gw},0}^{(2)}$ since ζ_{gL} is Gaussian. According to the Wick's theorem, the four-point correlator of ζ_{gL} therein leads to contractions at $\mathcal{O}(A_L^2)$ order with a Dirac δ function. Further, we use the line-of-sight relation $\mathbf{x} - \mathbf{x}' = (\eta_{\text{in}} - \eta_0)(\mathbf{n}_0 - \mathbf{n}'_0)$ and the identity $e^{ik\mu(\eta_{\text{in}} - \eta_0)} = 4\pi \sum_{\ell m} (-i)^\ell j_\ell[k(\eta_0 - \eta_{\text{in}})] Y_{\ell m}^*(\hat{\mathbf{k}}) Y_{\ell m}(\mathbf{n}_0)$ for subsequent calculations. By utilizing the representation of the Dirac δ function in terms of spherical harmonics and the orthonormality of spherical harmonics, the integral for $\tilde{b}_{\ell_1\ell_2\ell_3}(\nu)$ becomes

$$\tilde{b}_{\ell_1\ell_2\ell_3}(\nu) = \int_0^\infty dr r^2 \prod_{i=1}^3 \left[\frac{2}{\pi} \int_0^\infty dk_i k_i^2 j_{\ell_i}(k_i(\eta_0 - \eta_{\text{in}})) j_{\ell_i}(k_i r) \right] B(2\pi\nu, k_1, k_2, k_3) \quad (4.11)$$

where $B(q, k_1, k_2, k_3)$ is introduced by the three-point correlation of density contrast in Fourier mode, i.e.,

$$B(q, k_1, k_2, k_3) = 2 \left\{ \frac{\Omega_{\text{ng}}^{(1)}(\eta_{\text{in}}, q)}{\bar{\Omega}_{\text{gw}}(\eta_{\text{in}}, q)} + \frac{3}{5} \left[4 - n_{\text{gw}} \left(\frac{q}{2\pi} \right) \right] \right\}^2 \left\{ \frac{\Omega_{\text{ng}}^{(2)}(\eta_{\text{in}}, q)}{\bar{\Omega}_{\text{gw}}(\eta_{\text{in}}, q)} + \frac{9}{25} f_{\text{NL}} \left[4 - n_{\text{gw}} \left(\frac{q}{2\pi} \right) \right] \right\} \\ \times \left[\frac{2\pi^2}{k_1^3} \Delta_L^2(k_1) \frac{2\pi^2}{k_2^3} \Delta_L^2(k_2) + \frac{2\pi^2}{k_2^3} \Delta_L^2(k_2) \frac{2\pi^2}{k_3^3} \Delta_L^2(k_3) + \frac{2\pi^2}{k_3^3} \Delta_L^2(k_3) \frac{2\pi^2}{k_1^3} \Delta_L^2(k_1) \right]. \quad (4.12)$$

For simplicity, we set $\Delta_L^2 \simeq A_L$ in the following derivation. Further, by utilizing the closure relation of Bessel function

$$\frac{2}{\pi} \int_0^\infty dk k^2 j_\ell[k(\eta_0 - \eta_{\text{in}})] j_\ell(kr) = \frac{\delta(\eta_0 - \eta_{\text{in}} - r)}{r^2}, \quad (4.13)$$

and the integral of the form

$$\int_0^\infty d \ln k j_\ell^2(k(\eta_0 - \eta_{\text{in}})) = \frac{1}{2\ell(\ell + 1)}, \quad (4.14)$$

we can complete the integration of Eq. (4.11) and then get one of our leading results as follows

$$\tilde{b}_{\ell_1\ell_2\ell_3}(\nu) = b(\nu) \left[\frac{1}{\ell_1\ell_2(\ell_1 + 1)(\ell_2 + 1)} + \frac{1}{\ell_2\ell_3(\ell_2 + 1)(\ell_3 + 1)} + \frac{1}{\ell_3\ell_1(\ell_3 + 1)(\ell_1 + 1)} \right], \quad (4.15)$$

where we introduce a function $b(\nu)$ as follows

$$b(\nu) = 8\pi^2 A_L^2 \left\{ \frac{\Omega_{\text{ng}}^{(1)}(\eta_{\text{in}}, 2\pi\nu)}{\bar{\Omega}_{\text{gw}}(\eta_{\text{in}}, 2\pi\nu)} + \frac{3}{5} [4 - n_{\text{gw}}(\nu)] \right\}^2 \left\{ \frac{\Omega_{\text{ng}}^{(2)}(\eta_{\text{in}}, 2\pi\nu)}{\bar{\Omega}_{\text{gw}}(\eta_{\text{in}}, 2\pi\nu)} + \frac{9}{25} f_{\text{NL}} [4 - n_{\text{gw}}(\nu)] \right\}. \quad (4.16)$$

It is worth noting that Eqs. (4.3, 4.4, 4.16) imply that $b(\nu) = 0$ when $f_{\text{NL}} = g_{\text{NL}} = 0$. In other words, the Gaussian ζ always leads to a Gaussian background of SIGWs, which is in line with our expectation.

4.2 Angular trispectrum

Analogous to CMB [132], the reduced angular trispectrum $t_{\ell_3\ell_4}^{\ell_1\ell_2}(L, \nu)$ for SIGWs, as defined in Eqs. (3.10, 3.13, 3.14), can be obtained after a lengthy but similar derivation. As depicted in Figure 2, the non-vanishing connected contractions at the leading order in A_L correspond to two types of Feynman-like diagrams. One consists of two $\delta_{\text{gw},0}^{(2)}$ and two $\delta_{\text{gw},0}^{(1)}$ corresponding to the middle panel of Figure 2, while the other consists of one $\delta_{\text{gw},0}^{(3)}$ and three $\delta_{\text{gw},0}^{(1)}$ corresponding to the right panel of Figure 2. According to the permutation symmetry, $t_{\ell_3\ell_4}^{\ell_1\ell_2}(L, \nu)$ exactly corresponds to

$$\begin{aligned} & \frac{1}{2} \left\langle \delta_{\text{gw},0}^{(2)}(\mathbf{q}_1) \delta_{\text{gw},0}^{(1)}(\mathbf{q}_2) \delta_{\text{gw},0}^{(2)}(\mathbf{q}_3) \delta_{\text{gw},0}^{(1)}(\mathbf{q}_4) \right\rangle_c \\ & + \frac{1}{6} \left[\left\langle \delta_{\text{gw},0}^{(3)}(\mathbf{q}_1) \delta_{\text{gw},0}^{(1)}(\mathbf{q}_2) \delta_{\text{gw},0}^{(1)}(\mathbf{q}_3) \delta_{\text{gw},0}^{(1)}(\mathbf{q}_4) \right\rangle_c + \left\langle \delta_{\text{gw},0}^{(1)}(\mathbf{q}_1) \delta_{\text{gw},0}^{(1)}(\mathbf{q}_2) \delta_{\text{gw},0}^{(3)}(\mathbf{q}_3) \delta_{\text{gw},0}^{(1)}(\mathbf{q}_4) \right\rangle_c \right], \end{aligned}$$

where the subscript c denotes the connected part of the four-point correlators. The combination of these correlators in ℓ, m space can lead to

$$\begin{aligned} t_{\ell_3\ell_4}^{\ell_1\ell_2}(L, \nu) = & \left\{ 4 \left\{ \frac{\Omega_{\text{ng}}^{(1)}(\eta_{\text{in}}, 2\pi\nu)}{\bar{\Omega}_{\text{gw}}(\eta_{\text{in}}, 2\pi\nu)} + \frac{3}{5} [4 - n_{\text{gw}}(\nu)] \right\}^2 \left\{ \frac{\Omega_{\text{ng}}^{(2)}(\eta_{\text{in}}, 2\pi\nu)}{\bar{\Omega}_{\text{gw}}(\eta_{\text{in}}, 2\pi\nu)} + \frac{9}{25} f_{\text{NL}} [4 - n_{\text{gw}}(\nu)] \right\}^2 \right. \\ & \times \int dr_1 r_1^2 dr_2 r_2^2 F_L(r_1, r_2) \alpha_{\ell_1}(r_1) \beta_{\ell_2}(r_1) \alpha_{\ell_3}(r_2) \beta_{\ell_4}(r_2) \\ & + \frac{1}{4} \left\{ \frac{\Omega_{\text{ng}}^{(1)}(\eta_{\text{in}}, 2\pi\nu)}{\bar{\Omega}_{\text{gw}}(\eta_{\text{in}}, 2\pi\nu)} + \frac{3}{5} [4 - n_{\text{gw}}(\nu)] \right\}^3 \left\{ \frac{\Omega_{\text{ng}}^{(3)}(\eta_{\text{in}}, 2\pi\nu)}{\bar{\Omega}_{\text{gw}}(\eta_{\text{in}}, 2\pi\nu)} + \frac{27}{125} g_{\text{NL}} [4 - n_{\text{gw}}(\nu)] \right\} \\ & \left. \times \int r^2 dr [\alpha_{\ell_1}(r) \beta_{\ell_3}(r) + \beta_{\ell_1}(r) \alpha_{\ell_3}(r)] \beta_{\ell_2}(r) \beta_{\ell_4}(r) \right\} h_{\ell_1\ell_2L} h_{\ell_3\ell_4L}, \quad (4.17) \end{aligned}$$

where $h_{\ell\ell'\ell''}$ has been defined in Eq. (3.9), and we further introduce three integrals of the form

$$F_L(r_1, r_2) = 4\pi \int \frac{dK}{K} \Delta_{gL}(K) j_L(Kr_1) j_L(Kr_2), \quad (4.18)$$

$$\alpha_\ell(r) = \frac{2}{\pi} \int dk k^2 j_\ell(kr) j_\ell[k(\eta_0 - \eta_{\text{in}})], \quad (4.19)$$

$$\beta_\ell(r) = 4\pi \int \frac{dk}{k} \Delta_{gL}(k) j_\ell(kr) j_\ell[k(\eta_0 - \eta_{\text{in}})]. \quad (4.20)$$

In particular, for the scale-invariant $\Delta_{gL}(k) \simeq A_L$ considered in this work, we reduce $t_{\ell_3\ell_4}^{\ell_1\ell_2}(L, \nu)$ to

$$t_{\ell_3\ell_4}^{\ell_1\ell_2}(L, \nu) = \frac{1}{\ell_2(\ell_2 + 1)} \frac{1}{\ell_4(\ell_4 + 1)} \left[\frac{t_1(\nu)}{L(L + 1)} + \frac{t_2(\nu)}{\ell_1(\ell_1 + 1)} + \frac{t_3(\nu)}{\ell_3(\ell_3 + 1)} \right] h_{\ell_1\ell_2L} h_{\ell_3\ell_4L}, \quad (4.21)$$

where $t_1(\nu)$ and $t_2(\nu)$ are introduced as follows

$$t_1(\nu) = 4 \times (2\pi A_L)^3 \left\{ \frac{\Omega_{\text{ng}}^{(1)}(\eta_{\text{in}}, 2\pi\nu)}{\bar{\Omega}_{\text{gw}}(\eta_{\text{in}}, 2\pi\nu)} + \frac{3}{5} [4 - n_{\text{gw}}(\nu)] \right\}^2 \left\{ \frac{\Omega_{\text{ng}}^{(2)}(\eta_{\text{in}}, 2\pi\nu)}{\bar{\Omega}_{\text{gw}}(\eta_{\text{in}}, 2\pi\nu)} + \frac{9}{25} f_{\text{NL}} [4 - n_{\text{gw}}(\nu)] \right\}^2, \quad (4.22)$$

$$t_2(\nu) = \frac{(2\pi A_L)^3}{4} \left\{ \frac{\Omega_{\text{ng}}^{(1)}(\eta_{\text{in}}, 2\pi\nu)}{\bar{\Omega}_{\text{gw}}(\eta_{\text{in}}, 2\pi\nu)} + \frac{3}{5} [4 - n_{\text{gw}}(\nu)] \right\}^3 \left\{ \frac{\Omega_{\text{ng}}^{(3)}(\eta_{\text{in}}, 2\pi\nu)}{\bar{\Omega}_{\text{gw}}(\eta_{\text{in}}, 2\pi\nu)} + \frac{27}{125} g_{\text{NL}} [4 - n_{\text{gw}}(\nu)] \right\}. \quad (4.23)$$

It also stands for one of our leading results.

4.3 Frequency and multipole dependence

To investigate the frequency and multipole dependence for the angular bispectrum and trispectrum, we can reformulate $\tilde{b}_{\ell_1\ell_2\ell_3}(\nu)$ and $t_{\ell_3\ell_4}^{\ell_1\ell_2}(L, \nu)$ in terms of $\tilde{C}_\ell(\nu)$, namely

$$\begin{aligned} \tilde{b}_{\ell_1\ell_2\ell_3}(\nu) &= 2 \times \left[\frac{\Omega_{\text{ng}}^{(2)}}{\bar{\Omega}_{\text{gw}}} + \frac{9}{25} f_{\text{NL}} (4 - n_{\text{gw}}) \right] \left[\frac{\Omega_{\text{ng}}^{(1)}}{\bar{\Omega}_{\text{gw}}} + \frac{3}{5} (4 - n_{\text{gw}}) \right]^{-2} \\ &\quad \times \left(\tilde{C}_{\ell_1} \tilde{C}_{\ell_2} + \tilde{C}_{\ell_1} \tilde{C}_{\ell_3} + \tilde{C}_{\ell_2} \tilde{C}_{\ell_3} \right), \end{aligned} \quad (4.24)$$

$$\begin{aligned} t_{\ell_3\ell_4}^{\ell_1\ell_2}(L, \nu) &= \left\{ \left[\frac{\Omega_{\text{ng}}^{(3)}}{\bar{\Omega}_{\text{gw}}} + \frac{27}{125} g_{\text{NL}} (4 - n_{\text{gw}}) \right] \left[\frac{\Omega_{\text{ng}}^{(1)}}{\bar{\Omega}_{\text{gw}}} + \frac{3}{5} (4 - n_{\text{gw}}) \right]^{-5} (\tilde{C}_{\ell_1} + \tilde{C}_{\ell_3}) \right. \\ &\quad \left. + \left[\frac{\Omega_{\text{ng}}^{(2)}}{\bar{\Omega}_{\text{gw}}} + \frac{9}{25} f_{\text{NL}} (4 - n_{\text{gw}}) \right]^2 \left[\frac{\Omega_{\text{ng}}^{(1)}}{\bar{\Omega}_{\text{gw}}} + \frac{3}{5} (4 - n_{\text{gw}}) \right]^{-4} \tilde{C}_L \right\} h_{\ell_1\ell_2L} h_{\ell_3\ell_4L} \tilde{C}_{\ell_2} \tilde{C}_{\ell_4}. \end{aligned} \quad (4.25)$$

Here, $\tilde{C}_\ell(\nu)$ is already defined in Eq. (3.6) and its full analysis can be found in Ref. [25]. It is given by

$$\tilde{C}_\ell(\nu) = \frac{2\pi A_L}{\ell(\ell+1)} \left\{ \frac{\Omega_{\text{ng}}^{(1)}(\eta_{\text{in}}, 2\pi\nu)}{\bar{\Omega}_{\text{gw}}(\eta_{\text{in}}, 2\pi\nu)} + \frac{3}{5} [4 - n_{\text{gw}}(\nu)] \right\}^2. \quad (4.26)$$

We find that the frequency dependence is non-trivial, since Eqs. (4.24,4.26) are neither determined by the energy-density fraction spectrum nor the angular power spectrum. This implies that the angular bispectrum and trispectrum contains valuable information, which may be useful for extracting the SIGW signal from astrophysical foregrounds. It is worth noting that the above results differ from the existing works. The frequency dependence in the study of CMB is typically not considered due to the tightly couplings of particles in plasma, which is of thermal equilibrium in the early universe. As for a seminal work in Ref. [70], a fraction of contributions from f_{NL} to the angular bispectrum of SIGWs was considered, which, although frequency-dependent, can be uniquely determined by the angular power spectrum.

We also find that the multipole dependence for the angular bispectrum in Eq. (4.24) is uniquely determined by that of angular power spectrum. In contrast, the multipole dependence for the angular trispectrum in Eq. (4.26) is determined by those of angular power spectrum and $h_{\ell\ell'\ell''}$ which has been introduced by Eq. (3.9).

5 Numerical results

Based on the semi-analytic results in the former section, we can correspondingly display our numerical results in this section.

5.1 Angular bispectrum

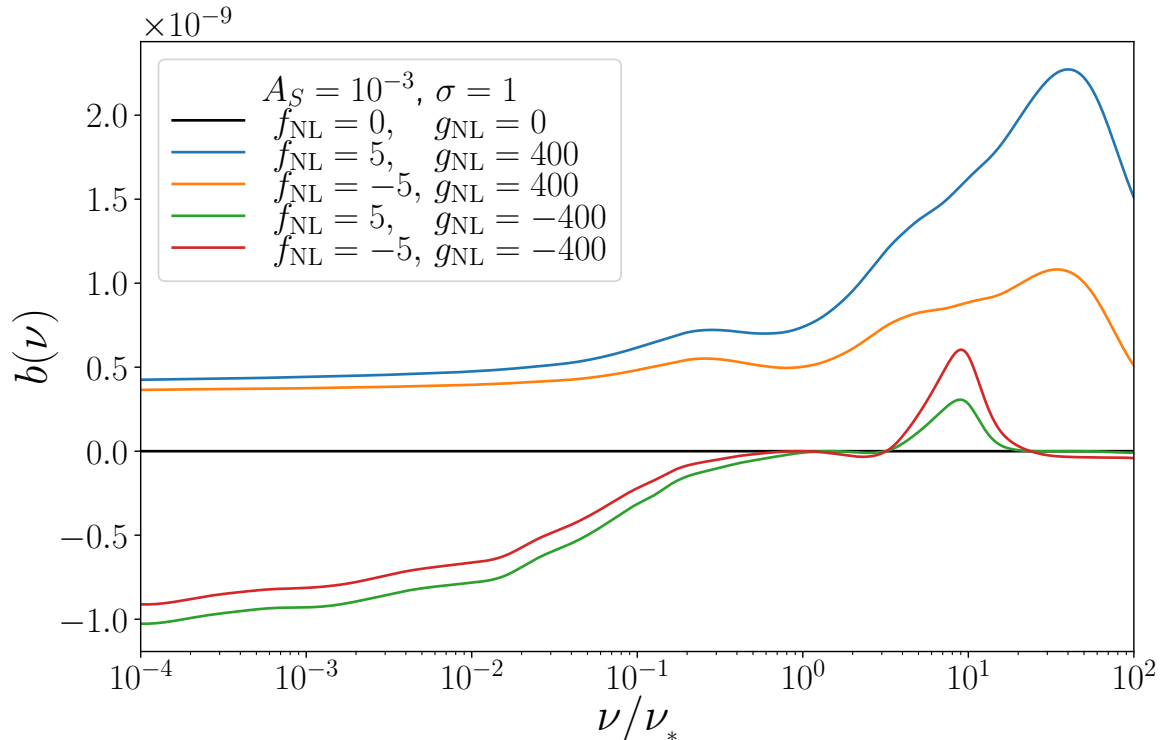


Figure 5: Frequency dependence of the reduced angular bispectrum of SIGWs.

While the multipole dependence of the reduced angular bispectrum, as shown in Eq. (4.15), is straightforward, we examine the function that characterizes the frequency dependence, denoted as $b(\nu)$ in Eq. (4.16). We numerically calculate $b(\nu)$ based on the numerical outcomes of $\bar{\Omega}_{\text{gw}}^{(a,b)}$ depicted in Figure 5 of Ref. [25], which is available for SIGWs produced during radiation domination. Assuming the primordial power spectrum for ζ_{gS} in Eq. (2.5) and fixing $\sigma = 1$, $b(\nu)$ becomes a function of the frequency ratio ν/ν_* , the amplitude A_S , as well as the non-Gaussian parameters f_{NL} and g_{NL} . Our numerical results are illustrated in Figure 5 and Figure 6.

Figure 5 illustrates the impact of non-Gaussian parameters on $b(\nu)$. For example, we compare the profiles of $f_{\text{NL}} = \pm 5$ and $g_{\text{NL}} = \pm 400$ with that of Gaussian ζ . The influence of $|f_{\text{NL}}|$ is observed to be more significant than that of $|g_{\text{NL}}|$, while the sign of g_{NL} has a more distinct impact on the profiles. As expected, the non-Gaussianity of SIGW background is caused by the non-Gaussian ζ while disappears for the Gaussian ζ which is denoted by the black line. However, the non-Gaussian ζ does not always lead to the non-Gaussianity of SIGW background across all frequency ranges. As presented by curves for $g_{\text{NL}} = -400$, which

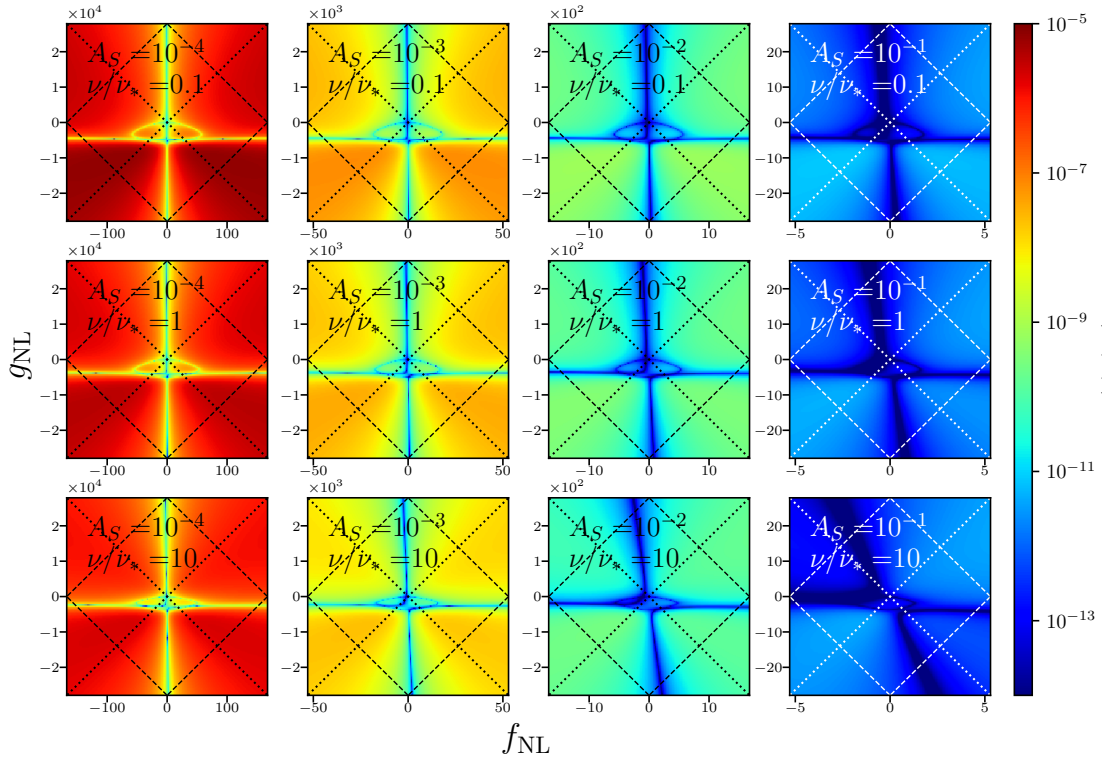


Figure 6: Frequency-dependent function for the reduced angular bispectrum of SIGWs with respect to the primordial non-Gaussian parameters f_{NL} and g_{NL} . Dotted lines represent $g_{\text{NL}} = \pm 5f_{\text{NL}}/(3\sqrt{A_S})$, which signify that the contribution from f_{NL} to ζ is equal to that from g_{NL} . Dashed lines represent $3|f_{\text{NL}}|\sqrt{A_S}/5 + 9|g_{\text{NL}}|A_S/25 = 1$, which signify that the contribution from non-Gaussian terms to ζ is equal to that from the Gaussian term.

are denoted as the green and red curves, $b(\nu)$ is nearly zero in the frequency band $\nu \sim \nu_*$. Moreover, for a negative g_{NL} , the angular bispectrum can be negative in lower-frequency ranges if the non-Gaussian parameters satisfy the conditions $(3g_{\text{NL}}A_S/5)^2 \lesssim f_{\text{NL}}^2A_S \lesssim 0.1$ approximately.

Figure 6 is an array constituting multiple contour plots with f_{NL} and g_{NL} as variables, obtained by selecting different values of A_S and ν/ν_* . It is presented to comprehensively elaborate the dependence of the SIGW angular bispectrum on f_{NL} and g_{NL} . Each panel is divided into four triangular regions by dotted lines, with the left and right regions representing the contribution from the g_{NL} term being smaller than that from the f_{NL} term, and the top and bottom regions representing the contribution from the g_{NL} term being larger than that from the f_{NL} term. It is worth noting that the value of the angular bispectrum within the “loop” in each panel is indeed negative. In other words, when g_{NL} is negative and both f_{NL} and $|g_{\text{NL}}|$ are relatively mild ($g_{\text{NL}} < 0$, $f_{\text{NL}}^2A_S \lesssim 0.25$, $-g_{\text{NL}}A_S \lesssim 0.5$), the angular bispectrum is negative. Additionally, larger $|f_{\text{NL}}|$ values or negative g_{NL} values typically result in larger bispectral amplitudes. Furthermore, a comparison across different panels reveals that larger values of A_S tend to decrease the reduced bispectral magnitude, whereas a small value of

A_S (10^{-4}) can lead to the value of the reduced bispectrum even up to 10^{-5} . As the same positions at each panel denote the same values of $f_{\text{NL}}\sqrt{A_S}$ and $g_{\text{NL}}A_S$, the comparison also implies that larger values of A_S or higher frequency ratio ν/ν_* generally suppress the effects from initial inhomogeneities relatively on the angular bispectrum.

5.2 Angular trispectrum

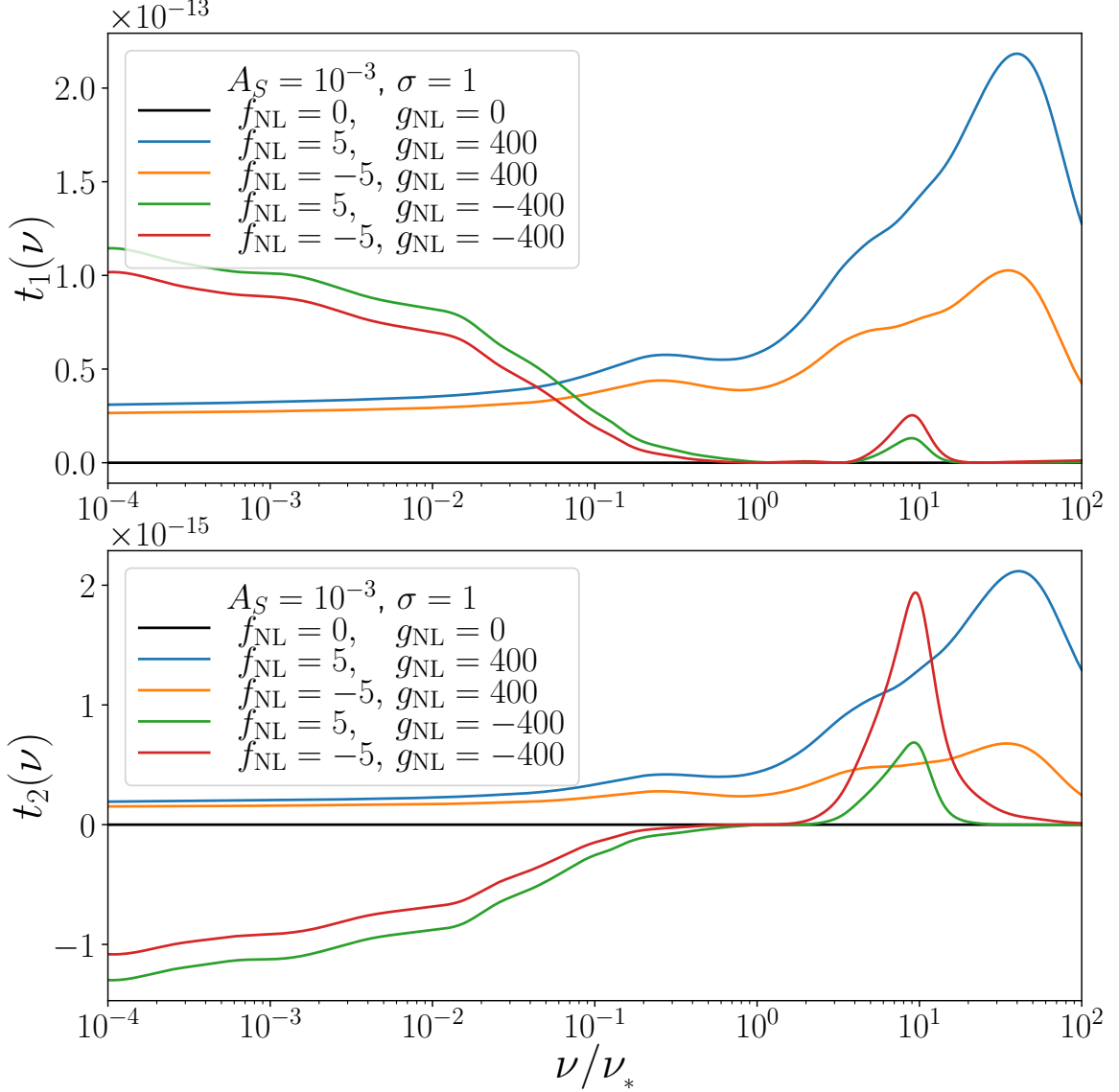


Figure 7: Frequency dependence of the reduced angular trispectrum of SIGWs.

Following the same step, we examine the two functions, defined as $t_1(\nu)$ in Eq. (4.22) and $t_2(\nu)$ in Eq. (4.23), that characterize the frequency dependence of the reduced angular trispectrum. Our numerical results are illustrated in Figure 7 and Figure 8.

Taking the same values of model parameters as in Figure 5, we compare the effects of different values of f_{NL} and g_{NL} as well as their signs on the above two functions in Figure 7.

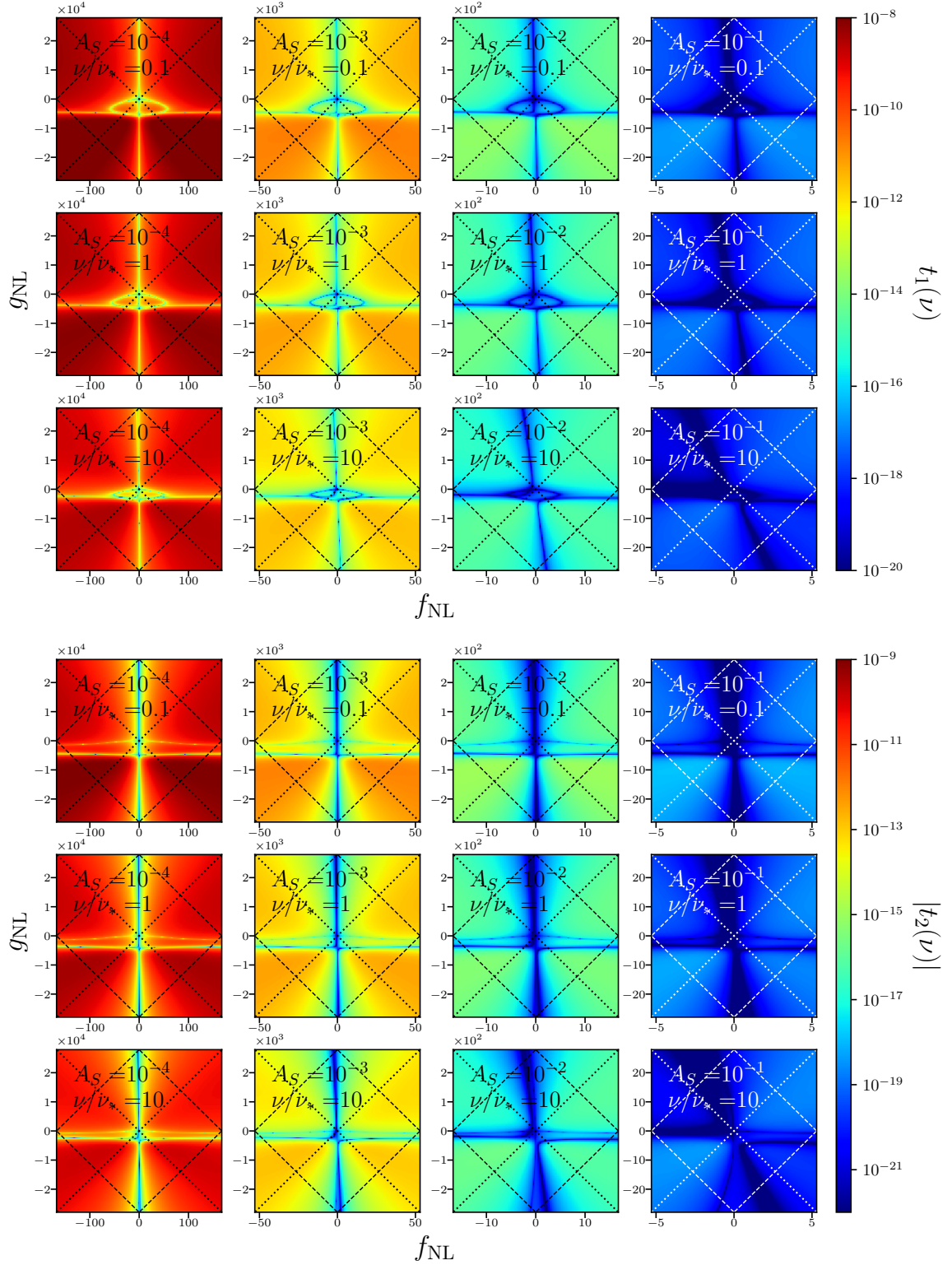


Figure 8: Frequency-dependent functions for the reduced angular trispectrum of SIGWs with respect to the primordial non-Gaussian parameters f_{NL} and g_{NL} . The conventions for the dotted and dashed lines are the same as those in Figure 6.

By construction, $t_1(\nu)$ and $b(\nu)$ behave similarly, apart from that $t_1(\nu)$ is always nonnegative and $t_1(\nu)/b(\nu) \sim \zeta_{gL}$. The upper panel of Figure 7 has met our expectation in comparison with Figure 5. For $t_2(\nu)$, its magnitude is nearly two orders of magnitude less than that of $t_1(\nu)$ for all the same sets of model parameters, though both $t_2(\nu)$ and $t_1(\nu)$ are of $\mathcal{O}(\zeta_{gL}^3)$ order. This suggests that the contributions from $\langle \delta_{\text{gw},0}^{(3)} \delta_{\text{gw},0}^{(1)} \delta_{\text{gw},0}^{(1)} \delta_{\text{gw},0}^{(1)} \rangle$ are subdominant in contrast with that from $\langle \delta_{\text{gw},0}^{(2)} \delta_{\text{gw},0}^{(2)} \delta_{\text{gw},0}^{(1)} \delta_{\text{gw},0}^{(1)} \rangle$. Moreover, $t_2(\nu)$ may take a negative value in the low-frequency range if the sign of g_{NL} is minus, which behaves distinctly from $t_1(\nu)$ but similarly to $b(\nu)$. The profiles of $t_2(\nu)$ are also influenced by $|f_{\text{NL}}|$ and the sign of g_{NL} mainly, which are identical to those of $b(\nu)$ and $t_1(\nu)$. In addition, similar to $b(\nu)$, the magnitudes of $t_1(\nu)$ and $t_2(\nu)$ are negligible at the frequency band $\nu \sim \nu_*$ when $g_{\text{NL}} = -400$.

We also depict two arrays for $t_1(\nu)$ and $|t_2(\nu)|$ in Figure 8, which are arranged identically to that of $b(\nu)$. We can read the dependence of the SIGW angular trispectrum on f_{NL} and g_{NL} easily from these arrays. While the contour plots of $t_1(\nu)$ are similar to those of $b(\nu)$ except the magnitudes and signs, the contour plots of $t_2(\nu)$ possess different features. It is observed that $t_2(\nu) < 0$ for a small value of $|g_{\text{NL}}|$ with a minus sign, regardless the value of f_{NL} . Additionally, for both $t_1(\nu)$ and $t_2(\nu)$, larger $|f_{\text{NL}}|$ values or negative g_{NL} values tend to increase their magnitudes while larger values of A_S always suppress them, which are same as that of $b(\nu)$. It is telling that the non-Gaussianity of SIGW background is more prominent in these cases. Though the magnitude of $t_2(\nu)$ is typically one order of magnitude smaller than that of $t_1(\nu)$, their different dependence on frequency and multipoles implies that the reduced angular trispectrum contains a wealth of information about the early universe.

6 Discussion and Conclusion

In this study, we have delved into the non-Gaussianity of SIGW background associated with the local-type primordial non-Gaussianity parameterized by f_{NL} and g_{NL} . For the first time, we have derived the explicit formulae for the angular bispectrum and trispectrum of SIGWs, which are complementary to our existing work [25] that devoted to the study of the energy-density fraction spectrum and angular power spectrum.

Based on the diagrammatic approach used in Ref. [25], we have generalized the computational technique to fully calculate the SIGW density contrast up to the $\mathcal{O}(A_L^3)$ order, and derived the comprehensive expressions for the reduced angular bispectrum $\tilde{b}_{\ell_1 \ell_2 \ell_3}(\nu)$ and trispectrum $t_{\ell_3 \ell_4}^{\ell_1 \ell_2}(L, \nu)$. Notably, these spectra were found to depend on frequency bands in a non-trivial way, as their information is unable to be compressed into the energy-density fraction spectrum $\Omega_{\text{gw},0}(\nu)$ and the reduced angular power spectrum $\tilde{C}_\ell(\nu)$. This suggests that the non-Gaussianity of SIGW background contains additional information about the SIGW background beyond the energy-density fraction spectrum and the angular power spectrum. Furthermore, the expressions for $\tilde{b}_{\ell_1 \ell_2 \ell_3}(\nu)$ and $t_{\ell_3 \ell_4}^{\ell_1 \ell_2}(L, \nu)$ have verified our prior expectation that the non-Gaussianity of SIGW background results from the primordial non-Gaussianity of cosmological curvature perturbations. Only when different modes of primordial curvature perturbations are coherent, SIGWs at two distant locations are coherent. We also found that for a negative value of g_{NL} , a positive SIGW angular bispectrum indicates significant primordial non-Gaussianity. Eventually, our numerical results reveal the substantial impact of

primordial non-Gaussianity on the angular bispectrum and trispectrum, with the bispectral amplitude reaching $\sim 10^{-5}$ and the trispectral amplitude reaching $\sim 10^{-8}$ for specific sets of model parameters.

The future advancements in the angular resolution of GW detectors will allow possible extractions of valuable information from the detection of the stochastic GW background, which can be produced from the superposition of various sources. Recently, multiple pulsar timing array (PTA) experiments [140–143] have announced the existence of a stochastic GW background with compelling evidence. However, the datasets did not affirm a certain GW source for the signal, with various possibilities discussed by accompanying papers [144, 145]. Subsequent studies [72, 146–183] speculated that this signal potentially originates from SIGWs. The authors provided an avenue for testing and validating the presence of SIGWs and the associated non-Gaussian features. In particular, Refs. [25, 72] showed that if the PTA signal originates from SIGWs, it can be tested with the Square Kilometre Array (SKA) [45–47] by measuring the corresponding angular power spectrum. If the angular resolution of SKA is sufficient enough to observe the anisotropies in the stochastic GW background, there is a promising opportunity to measure its angular bispectrum and trispectrum, besides the energy-density fraction spectrum and the angular power spectrum, thereby further confirming the sources of the signal and even determining the relevant model parameters.

Our present study would be helpful in search of PBHs, which are hypothesized to be a reasonable candidate of cold dark matter and a potential origin of the individual GW events observed by the Advanced LIGO, Virgo, and KAGRA [184–188]. As emphasized in the prior works [51, 52, 77–98], the mass function of PBHs is significantly influenced by the presence of primordial non-Gaussianity, as their formation threshold can be affected by specific characteristics of the non-Gaussianity. It is worth noting that the angular bispectrum and trispectrum of SIGW background are also significantly affected by the primordial power spectrum. Therefore, future measurements of the non-Gaussianity of this SIGW background may further exert constraints on the PBH scenarios. In addition, the couplings between short- and long-wavelength modes also cause an inhomogeneous distribution of PBHs on large scales [189]. If PBHs contribute to dark matter, the primordial non-Gaussianity produces the isocurvature perturbations of dark matter during radiation domination [80, 190]. The CMB constraints on these isocurvature modes from the `Planck` satellite [191] could impose limits on the local-type primordial non-Gaussianity [70, 112]. They are expected to be further enhanced by future observations of CMB and LSS. We would not delve into a detailed study of them in this work, but defer it to future works.

In this work, we have focused on local-type primordial non-Gaussianity with scale-invariance, but our approach can be extended to more general cases. For clarification, the energy-density fraction spectrum is sensitive to the primordial non-Gaussianity on small scales, while the anisotropy is related with the primordial non-Gaussianity that characterize couplings between short- and long-wavelength curvature perturbations, although we treat them as the same in this work. If f_{NL} and g_{NL} change gradually across frequency bands, we can treat them as constants when evaluating the energy-density fraction spectrum and simply use varying values in the numerators in Eqs. (4.3,4.4,4.5), similar to the method used in Ref. [57]. Otherwise, if the scale-dependence of f_{NL} and g_{NL} is non-negligible in the

relevant frequency bands, we would need to incorporate them into the integrands for the components of energy-density fraction spectrum and integrate these integrands as a whole, which would significantly complicate the numerical calculation though the semi-analytical expressions are similar. It is worth noting that this method is also available beyond the postulation of local-type, which has been adopted in Ref. [54]. Moreover, other shapes of primordial non-Gaussianity, rather than the local-type considered in our present work, are unlikely to cause significant anisotropy and non-Gaussianity of SIGW background, as the deviations from isotropic and Gaussian SIGW background stem from the couplings between short- and long-wavelength modes.

In conclusion, our work is of great significance for future detection of stochastic GW background and exploration of the early universe and dark matter. Measurements of angular bispectrum and trispectrum of stochastic GW background would provide a vital complement to probe the primordial non-Gaussianity beyond the sensitive regimes of CMB and LSS. We would like to highlight that our research approach can be easily extended to study the primordial non-Gaussianity of higher orders than g_{NL} or with the scale-dependence.

Acknowledgments

We appreciate Mr. Yan-Heng Yu for helpful discussion. S.W. and J.P.L. are partially supported by the National Natural Science Foundation of China (Grant No. 12175243), the National Key R&D Program of China No. 2023YFC2206403, the Science Research Grants from the China Manned Space Project with No. CMS-CSSST-2021-B01, and the Key Research Program of the Chinese Academy of Sciences (Grant No. XDPB15). Z.C.Z. is supported by the National Key Research and Development Program of China Grant No. 2021YFC2203001 and the National Natural Science Foundation of China (Grant NO. 12005016). K.K. is supported by KAKENHI Grant No. JP22H05270.

References

- [1] J.M. Maldacena, *Non-Gaussian features of primordial fluctuations in single field inflationary models*, *JHEP* **05** (2003) 013 [[astro-ph/0210603](#)].
- [2] N. Bartolo, E. Komatsu, S. Matarrese and A. Riotto, *Non-Gaussianity from inflation: Theory and observations*, *Phys. Rept.* **402** (2004) 103 [[astro-ph/0406398](#)].
- [3] T.J. Allen, B. Grinstein and M.B. Wise, *Nongaussian Density Perturbations in Inflationary Cosmologies*, *Phys. Lett. B* **197** (1987) 66.
- [4] N. Bartolo, S. Matarrese and A. Riotto, *Nongaussianity from inflation*, *Phys. Rev. D* **65** (2002) 103505 [[hep-ph/0112261](#)].
- [5] V. Acquaviva, N. Bartolo, S. Matarrese and A. Riotto, *Second order cosmological perturbations from inflation*, *Nucl. Phys. B* **667** (2003) 119 [[astro-ph/0209156](#)].
- [6] F. Bernardeau and J.-P. Uzan, *NonGaussianity in multifield inflation*, *Phys. Rev. D* **66** (2002) 103506 [[hep-ph/0207295](#)].
- [7] X. Chen, M.-x. Huang, S. Kachru and G. Shiu, *Observational signatures and non-Gaussianities of general single field inflation*, *JCAP* **01** (2007) 002 [[hep-th/0605045](#)].

- [8] D.S. Salopek, J.R. Bond and J.M. Bardeen, *Designing Density Fluctuation Spectra in Inflation*, *Phys. Rev. D* **40** (1989) 1753.
- [9] D.H. Lyth and A. Riotto, *Particle physics models of inflation and the cosmological density perturbation*, *Phys. Rept.* **314** (1999) 1 [[hep-ph/9807278](#)].
- [10] P.D. Meerburg et al., *Primordial Non-Gaussianity*, [1903.04409](#).
- [11] J. Smidt, A. Amblard, C.T. Byrnes, A. Cooray, A. Heavens and D. Munshi, *CMB Constraints on Primordial non-Gaussianity from the Bispectrum (f_{NL}) and Trispectrum (g_{NL} and τ_{NL}) and a New Consistency Test of Single-Field Inflation*, *Phys. Rev. D* **81** (2010) 123007 [[1004.1409](#)].
- [12] PLANCK collaboration, *Planck 2018 results. IX. Constraints on primordial non-Gaussianity*, *Astron. Astrophys.* **641** (2020) A9 [[1905.05697](#)].
- [13] E. Castorina et al., *Redshift-weighted constraints on primordial non-Gaussianity from the clustering of the eBOSS DR14 quasars in Fourier space*, *JCAP* **09** (2019) 010 [[1904.08859](#)].
- [14] M. Biagetti, A. Cole and G. Shiu, *The Persistence of Large Scale Structures I: Primordial non-Gaussianity*, *JCAP* **04** (2021) 061 [[2009.04819](#)].
- [15] S. Dodelson, *Modern Cosmology*, Academic Press, Amsterdam (2003).
- [16] N. Bartolo, A. Hoseinpour, G. Orlando, S. Matarrese and M. Zarei, *Photon-graviton scattering: A new way to detect anisotropic gravitational waves?*, *Phys. Rev. D* **98** (2018) 023518 [[1804.06298](#)].
- [17] R. Flauger and S. Weinberg, *Absorption of Gravitational Waves from Distant Sources*, *Phys. Rev. D* **99** (2019) 123030 [[1906.04853](#)].
- [18] K.N. Ananda, C. Clarkson and D. Wands, *The Cosmological gravitational wave background from primordial density perturbations*, *Phys. Rev. D* **75** (2007) 123518 [[gr-qc/0612013](#)].
- [19] D. Baumann, P.J. Steinhardt, K. Takahashi and K. Ichiki, *Gravitational Wave Spectrum Induced by Primordial Scalar Perturbations*, *Phys. Rev. D* **76** (2007) 084019 [[hep-th/0703290](#)].
- [20] J.R. Espinosa, D. Racco and A. Riotto, *A Cosmological Signature of the SM Higgs Instability: Gravitational Waves*, *JCAP* **09** (2018) 012 [[1804.07732](#)].
- [21] K. Kohri and T. Terada, *Semianalytic calculation of gravitational wave spectrum nonlinearly induced from primordial curvature perturbations*, *Phys. Rev. D* **97** (2018) 123532 [[1804.08577](#)].
- [22] S. Mollerach, D. Harari and S. Matarrese, *CMB polarization from secondary vector and tensor modes*, *Phys. Rev. D* **69** (2004) 063002 [[astro-ph/0310711](#)].
- [23] H. Assadullahi and D. Wands, *Constraints on primordial density perturbations from induced gravitational waves*, *Phys. Rev. D* **81** (2010) 023527 [[0907.4073](#)].
- [24] G. Domènech, *Scalar Induced Gravitational Waves Review*, *Universe* **7** (2021) 398 [[2109.01398](#)].
- [25] J.-P. Li, S. Wang, Z.-C. Zhao and K. Kohri, *Complete Analysis of Scalar-Induced Gravitational Waves and Primordial Non-Gaussianities f_{NL} and g_{NL}* , [2309.07792](#).
- [26] J. Baker et al., *The Laser Interferometer Space Antenna: Unveiling the Millihertz Gravitational Wave Sky*, [1907.06482](#).

- [27] T.L. Smith, T.L. Smith, R.R. Caldwell and R. Caldwell, *LISA for Cosmologists: Calculating the Signal-to-Noise Ratio for Stochastic and Deterministic Sources*, *Phys. Rev. D* **100** (2019) 104055 [[1908.00546](#)].
- [28] W.-R. Hu and Y.-L. Wu, *The Taiji Program in Space for gravitational wave physics and the nature of gravity*, *Natl. Sci. Rev.* **4** (2017) 685.
- [29] G. Wang and W.-B. Han, *Alternative LISA-TAIJI networks: Detectability of the isotropic stochastic gravitational wave background*, *Phys. Rev. D* **104** (2021) 104015 [[2108.11151](#)].
- [30] Z. Ren, T. Zhao, Z. Cao, Z.-K. Guo, W.-B. Han, H.-B. Jin et al., *Taiji data challenge for exploring gravitational wave universe*, *Front. Phys. (Beijing)* **18** (2023) 64302 [[2301.02967](#)].
- [31] TIANQIN collaboration, *TianQin: a space-borne gravitational wave detector*, *Class. Quant. Grav.* **33** (2016) 035010 [[1512.02076](#)].
- [32] TIANQIN collaboration, *The TianQin project: current progress on science and technology*, *PTEP* **2021** (2021) 05A107 [[2008.10332](#)].
- [33] N. Seto, S. Kawamura and T. Nakamura, *Possibility of direct measurement of the acceleration of the universe using 0.1-Hz band laser interferometer gravitational wave antenna in space*, *Phys. Rev. Lett.* **87** (2001) 221103 [[astro-ph/0108011](#)].
- [34] S. Kawamura et al., *Current status of space gravitational wave antenna DECIGO and B-DECIGO*, *PTEP* **2021** (2021) 05A105 [[2006.13545](#)].
- [35] J. Crowder and N.J. Cornish, *Beyond LISA: Exploring future gravitational wave missions*, *Phys. Rev. D* **72** (2005) 083005 [[gr-qc/0506015](#)].
- [36] T.L. Smith and R. Caldwell, *Sensitivity to a Frequency-Dependent Circular Polarization in an Isotropic Stochastic Gravitational Wave Background*, *Phys. Rev. D* **95** (2017) 044036 [[1609.05901](#)].
- [37] G. Capurri, A. Lapi, L. Boco and C. Baccigalupi, *Searching for Anisotropic Stochastic Gravitational-wave Backgrounds with Constellations of Space-based Interferometers*, *Astrophys. J.* **943** (2023) 72 [[2212.06162](#)].
- [38] G. Hobbs et al., *The international pulsar timing array project: using pulsars as a gravitational wave detector*, *Class. Quant. Grav.* **27** (2010) 084013 [[0911.5206](#)].
- [39] P.B. Demorest et al., *Limits on the Stochastic Gravitational Wave Background from the North American Nanohertz Observatory for Gravitational Waves*, *Astrophys. J.* **762** (2013) 94 [[1201.6641](#)].
- [40] EPTA collaboration, *The European Pulsar Timing Array and the Large European Array for Pulsars*, *Class. Quant. Grav.* **30** (2013) 224009.
- [41] R.N. Manchester et al., *The Parkes Pulsar Timing Array Project*, *Publ. Astron. Soc. Austral.* **30** (2013) 17 [[1210.6130](#)].
- [42] A. Sesana, A. Vecchio and C.N. Colacino, *The stochastic gravitational-wave background from massive black hole binary systems: implications for observations with Pulsar Timing Arrays*, *Mon. Not. Roy. Astron. Soc.* **390** (2008) 192 [[0804.4476](#)].
- [43] E. Thrane and J.D. Romano, *Sensitivity curves for searches for gravitational-wave backgrounds*, *Phys. Rev. D* **88** (2013) 124032 [[1310.5300](#)].
- [44] G. Janssen et al., *Gravitational wave astronomy with the SKA*, *PoS AASKA14* (2015) 037 [[1501.00127](#)].

- [45] P.E. Dewdney, P.J. Hall, R.T. Schilizzi and T.J.L.W. Lazio, *The Square Kilometre Array*, *IEEE Proceedings* **97** (2009) 1482.
- [46] A. Weltman et al., *Fundamental physics with the Square Kilometre Array*, *Publ. Astron. Soc. Austral.* **37** (2020) e002 [[1810.02680](#)].
- [47] C.J. Moore, R.H. Cole and C.P.L. Berry, *Gravitational-wave sensitivity curves*, *Class. Quant. Grav.* **32** (2015) 015014 [[1408.0740](#)].
- [48] KAGRA, LIGO SCIENTIFIC, VIRGO, VIRGO collaboration, *Prospects for observing and localizing gravitational-wave transients with Advanced LIGO, Advanced Virgo and KAGRA*, *Living Rev. Rel.* **21** (2018) 3 [[1304.0670](#)].
- [49] LIGO SCIENTIFIC collaboration, *Advanced LIGO*, *Class. Quant. Grav.* **32** (2015) 074001 [[1411.4547](#)].
- [50] Z.-C. Chen, C. Yuan and Q.-G. Huang, *Confronting the primordial black hole scenario with the gravitational-wave events detected by LIGO-Virgo*, *Phys. Lett. B* **829** (2022) 137040 [[2108.11740](#)].
- [51] T. Nakama, J. Silk and M. Kamionkowski, *Stochastic gravitational waves associated with the formation of primordial black holes*, *Phys. Rev. D* **95** (2017) 043511 [[1612.06264](#)].
- [52] J. Garcia-Bellido, M. Peloso and C. Unal, *Gravitational Wave signatures of inflationary models from Primordial Black Hole Dark Matter*, *JCAP* **09** (2017) 013 [[1707.02441](#)].
- [53] P. Adshead, K.D. Lozanov and Z.J. Weiner, *Non-Gaussianity and the induced gravitational wave background*, *JCAP* **10** (2021) 080 [[2105.01659](#)].
- [54] H.V. Ragavendra, *Accounting for scalar non-Gaussianity in secondary gravitational waves*, *Phys. Rev. D* **105** (2022) 063533 [[2108.04193](#)].
- [55] K.T. Abe, R. Inui, Y. Tada and S. Yokoyama, *Primordial black holes and gravitational waves induced by exponential-tailed perturbations*, *JCAP* **05** (2023) 044 [[2209.13891](#)].
- [56] C. Yuan, D.-S. Meng and Q.-G. Huang, *Full analysis of the scalar-induced gravitational waves for the curvature perturbation with local-type non-Gaussianities*, *JCAP* **12** (2023) 036 [[2308.07155](#)].
- [57] Y.-H. Yu and S. Wang, *Anisotropies in Scalar-Induced Gravitational-Wave Background from Inflaton-Curvaton Mixed Scenario with Sound Speed Resonance*, [2310.14606](#).
- [58] H.V. Ragavendra, P. Saha, L. Sriramkumar and J. Silk, *Primordial black holes and secondary gravitational waves from ultraslow roll and punctuated inflation*, *Phys. Rev. D* **103** (2021) 083510 [[2008.12202](#)].
- [59] S. Garcia-Saenz, L. Pinol, S. Renaux-Petel and D. Werth, *No-go theorem for scalar-trispectrum-induced gravitational waves*, *JCAP* **03** (2023) 057 [[2207.14267](#)].
- [60] R.-g. Cai, S. Pi and M. Sasaki, *Gravitational Waves Induced by non-Gaussian Scalar Perturbations*, *Phys. Rev. Lett.* **122** (2019) 201101 [[1810.11000](#)].
- [61] C. Unal, *Imprints of Primordial Non-Gaussianity on Gravitational Wave Spectrum*, *Phys. Rev. D* **99** (2019) 041301 [[1811.09151](#)].
- [62] V. Atal and G. Domènech, *Probing non-Gaussianities with the high frequency tail of induced gravitational waves*, *JCAP* **06** (2021) 001 [[2103.01056](#)].
- [63] C. Yuan and Q.-G. Huang, *Gravitational waves induced by the local-type non-Gaussian curvature perturbations*, *Phys. Lett. B* **821** (2021) 136606 [[2007.10686](#)].

- [64] F. Zhang, *Primordial black holes and scalar induced gravitational waves from the E model with a Gauss-Bonnet term*, *Phys. Rev. D* **105** (2022) 063539 [[2112.10516](#)].
- [65] C. Yuan and Q.-G. Huang, *A topic review on probing primordial black hole dark matter with scalar induced gravitational waves*, [2103.04739](#).
- [66] J. Lin, S. Gao, Y. Gong, Y. Lu, Z. Wang and F. Zhang, *Primordial black holes and scalar induced gravitational waves from Higgs inflation with noncanonical kinetic term*, *Phys. Rev. D* **107** (2023) 043517 [[2111.01362](#)].
- [67] L.-Y. Chen, H. Yu and P. Wu, *Primordial non-Gaussianity in inflation with gravitationally enhanced friction*, *Phys. Rev. D* **106** (2022) 063537 [[2210.05201](#)].
- [68] R.-G. Cai, S. Pi, S.-J. Wang and X.-Y. Yang, *Resonant multiple peaks in the induced gravitational waves*, *JCAP* **05** (2019) 013 [[1901.10152](#)].
- [69] R.-G. Cai, S. Pi, S.-J. Wang and X.-Y. Yang, *Pulsar Timing Array Constraints on the Induced Gravitational Waves*, *JCAP* **10** (2019) 059 [[1907.06372](#)].
- [70] N. Bartolo, D. Bertacca, V. De Luca, G. Franciolini, S. Matarrese, M. Peloso et al., *Gravitational wave anisotropies from primordial black holes*, *JCAP* **02** (2020) 028 [[1909.12619](#)].
- [71] J.-P. Li, S. Wang, Z.-C. Zhao and K. Kohri, *Primordial non-Gaussianity f_{NL} and anisotropies in scalar-induced gravitational waves*, *JCAP* **10** (2023) 056 [[2305.19950](#)].
- [72] S. Wang, Z.-C. Zhao, J.-P. Li and Q.-H. Zhu, *Exploring the Implications of 2023 Pulsar Timing Array Datasets for Scalar-Induced Gravitational Waves and Primordial Black Holes*, [2307.00572](#).
- [73] S. Hawking, *Gravitationally collapsed objects of very low mass*, *Mon. Not. Roy. Astron. Soc.* **152** (1971) 75.
- [74] M. Sasaki, T. Suyama, T. Tanaka and S. Yokoyama, *Primordial black holes—perspectives in gravitational wave astronomy*, *Class. Quant. Grav.* **35** (2018) 063001 [[1801.05235](#)].
- [75] B. Carr and F. Kuhnel, *Primordial Black Holes as Dark Matter: Recent Developments*, *Ann. Rev. Nucl. Part. Sci.* **70** (2020) 355 [[2006.02838](#)].
- [76] B. Carr, S. Clesse, J. Garcia-Bellido, M. Hawkins and F. Kuhnel, *Observational evidence for primordial black holes: A positivist perspective*, *Phys. Rept.* **1054** (2024) 1 [[2306.03903](#)].
- [77] J.S. Bullock and J.R. Primack, *NonGaussian fluctuations and primordial black holes from inflation*, *Phys. Rev. D* **55** (1997) 7423 [[astro-ph/9611106](#)].
- [78] C.T. Byrnes, E.J. Copeland and A.M. Green, *Primordial black holes as a tool for constraining non-Gaussianity*, *Phys. Rev. D* **86** (2012) 043512 [[1206.4188](#)].
- [79] S. Young and C.T. Byrnes, *Primordial black holes in non-Gaussian regimes*, *JCAP* **08** (2013) 052 [[1307.4995](#)].
- [80] G. Franciolini, A. Kehagias, S. Matarrese and A. Riotto, *Primordial Black Holes from Inflation and non-Gaussianity*, *JCAP* **03** (2018) 016 [[1801.09415](#)].
- [81] S. Passaglia, W. Hu and H. Motohashi, *Primordial black holes and local non-Gaussianity in canonical inflation*, *Phys. Rev. D* **99** (2019) 043536 [[1812.08243](#)].
- [82] V. Atal and C. Germani, *The role of non-gaussianities in Primordial Black Hole formation*, *Phys. Dark Univ.* **24** (2019) 100275 [[1811.07857](#)].

- [83] V. Atal, J. Garriga and A. Marcos-Caballero, *Primordial black hole formation with non-Gaussian curvature perturbations*, *JCAP* **09** (2019) 073 [[1905.13202](#)].
- [84] M. Taoso and A. Urbano, *Non-gaussianities for primordial black hole formation*, *JCAP* **08** (2021) 016 [[2102.03610](#)].
- [85] D.-S. Meng, C. Yuan and Q.-g. Huang, *One-loop correction to the enhanced curvature perturbation with local-type non-Gaussianity for the formation of primordial black holes*, *Phys. Rev. D* **106** (2022) 063508 [[2207.07668](#)].
- [86] C. Chen, A. Ghoshal, Z. Lalak, Y. Luo and A. Naskar, *Growth of curvature perturbations for PBH formation in non-minimal curvaton scenario revisited*, [2305.12325](#).
- [87] R. Kawaguchi, T. Fujita and M. Sasaki, *Highly asymmetric probability distribution from a finite-width upward step during inflation*, [2305.18140](#).
- [88] C. Fu, P. Wu and H. Yu, *Primordial black holes and oscillating gravitational waves in slow-roll and slow-climb inflation with an intermediate noninflationary phase*, *Phys. Rev. D* **102** (2020) 043527 [[2006.03768](#)].
- [89] K. Inomata, M. Kawasaki, K. Mukaida and T.T. Yanagida, *NANOGrav Results and LIGO-Virgo Primordial Black Holes in Axionlike Curvaton Models*, *Phys. Rev. Lett.* **126** (2021) 131301 [[2011.01270](#)].
- [90] S. Young, C.T. Byrnes and M. Sasaki, *Calculating the mass fraction of primordial black holes*, *JCAP* **07** (2014) 045 [[1405.7023](#)].
- [91] S. Choudhury, A. Karde, S. Panda and M. Sami, *Primordial non-Gaussianity from ultra slow-roll Galileon inflation*, [2306.12334](#).
- [92] G. Ferrante, G. Franciolini, A. Iovino, Junior. and A. Urbano, *Primordial non-Gaussianity up to all orders: Theoretical aspects and implications for primordial black hole models*, *Phys. Rev. D* **107** (2023) 043520 [[2211.01728](#)].
- [93] A.M. Green and B.J. Kavanagh, *Primordial Black Holes as a dark matter candidate*, *J. Phys. G* **48** (2021) 043001 [[2007.10722](#)].
- [94] B. Carr, K. Kohri, Y. Sendouda and J. Yokoyama, *Constraints on primordial black holes*, *Rept. Prog. Phys.* **84** (2021) 116902 [[2002.12778](#)].
- [95] A. Escrivà, F. Kuhnel and Y. Tada, *Primordial Black Holes*, [2211.05767](#).
- [96] A. Escrivà, Y. Tada, S. Yokoyama and C.-M. Yoo, *Simulation of primordial black holes with large negative non-Gaussianity*, *JCAP* **05** (2022) 012 [[2202.01028](#)].
- [97] J.M. Ezquiaga, J. García-Bellido and V. Vennin, *The exponential tail of inflationary fluctuations: consequences for primordial black holes*, *JCAP* **03** (2020) 029 [[1912.05399](#)].
- [98] A. Kehagias, I. Musco and A. Riotto, *Non-Gaussian Formation of Primordial Black Holes: Effects on the Threshold*, *JCAP* **12** (2019) 029 [[1906.07135](#)].
- [99] Y.-F. Cai, X.-H. Ma, M. Sasaki, D.-G. Wang and Z. Zhou, *One small step for an inflaton, one giant leap for inflation: A novel non-Gaussian tail and primordial black holes*, *Phys. Lett. B* **834** (2022) 137461 [[2112.13836](#)].
- [100] Y.-F. Cai, X.-H. Ma, M. Sasaki, D.-G. Wang and Z. Zhou, *Highly non-Gaussian tails and primordial black holes from single-field inflation*, *JCAP* **12** (2022) 034 [[2207.11910](#)].

- [101] Z. Yi, Q. Gao, Y. Gong and Z.-h. Zhu, *Primordial black holes and scalar-induced secondary gravitational waves from inflationary models with a noncanonical kinetic term*, *Phys. Rev. D* **103** (2021) 063534 [[2011.10606](#)].
- [102] F. Zhang, J. Lin and Y. Lu, *Double-peaked inflation model: Scalar induced gravitational waves and primordial-black-hole suppression from primordial non-Gaussianity*, *Phys. Rev. D* **104** (2021) 063515 [[2106.10792](#)].
- [103] N. Bartolo, D. Bertacca, S. Matarrese, M. Peloso, A. Ricciardone, A. Riotto et al., *Anisotropies and non-Gaussianity of the Cosmological Gravitational Wave Background*, *Phys. Rev. D* **100** (2019) 121501 [[1908.00527](#)].
- [104] N. Bartolo, D. Bertacca, S. Matarrese, M. Peloso, A. Ricciardone, A. Riotto et al., *Characterizing the cosmological gravitational wave background: Anisotropies and non-Gaussianity*, *Phys. Rev. D* **102** (2020) 023527 [[1912.09433](#)].
- [105] N. Bartolo, V. Domcke, D.G. Figueroa, J. García-Bellido, M. Peloso, M. Pieroni et al., *Probing non-Gaussian Stochastic Gravitational Wave Backgrounds with LISA*, *JCAP* **11** (2018) 034 [[1806.02819](#)].
- [106] N. Bartolo, V. De Luca, G. Franciolini, A. Lewis, M. Peloso and A. Riotto, *Primordial Black Hole Dark Matter: LISA Serendipity*, *Phys. Rev. Lett.* **122** (2019) 211301 [[1810.12218](#)].
- [107] N. Bartolo, V. De Luca, G. Franciolini, M. Peloso, D. Racco and A. Riotto, *Testing primordial black holes as dark matter with LISA*, *Phys. Rev. D* **99** (2019) 103521 [[1810.12224](#)].
- [108] J.-Q. Jiang and Y.-S. Piao, *Search for the non-linearities of gravitational wave background in NANOGrav 15-year data set*, [2401.16950](#).
- [109] Q.-H. Zhu, *Intrinsic bispectrum of the scalar-induced gravitational waves*, [2402.02353](#).
- [110] E. Komatsu and D.N. Spergel, *Acoustic signatures in the primary microwave background bispectrum*, *Phys. Rev. D* **63** (2001) 063002 [[astro-ph/0005036](#)].
- [111] T. Okamoto and W. Hu, *The angular trispectra of CMB temperature and polarization*, *Phys. Rev. D* **66** (2002) 063008 [[astro-ph/0206155](#)].
- [112] Y. Tada and S. Yokoyama, *Primordial black holes as biased tracers*, *Phys. Rev. D* **91** (2015) 123534 [[1502.01124](#)].
- [113] PLANCK collaboration, *Planck 2018 results. VI. Cosmological parameters*, *Astron. Astrophys.* **641** (2020) A6 [[1807.06209](#)].
- [114] M. Maggiore, *Gravitational wave experiments and early universe cosmology*, *Phys. Rept.* **331** (2000) 283 [[gr-qc/9909001](#)].
- [115] S. Wang, T. Terada and K. Kohri, *Prospective constraints on the primordial black hole abundance from the stochastic gravitational-wave backgrounds produced by coalescing events and curvature perturbations*, *Phys. Rev. D* **99** (2019) 103531 [[1903.05924](#)].
- [116] C.R. Contaldi, *Anisotropies of Gravitational Wave Backgrounds: A Line Of Sight Approach*, *Phys. Lett. B* **771** (2017) 9 [[1609.08168](#)].
- [117] R.K. Sachs and A.M. Wolfe, *Perturbations of a cosmological model and angular variations of the microwave background*, *Astrophys. J.* **147** (1967) 73.
- [118] L. Valbusa Dall’Armi, A. Ricciardone, N. Bartolo, D. Bertacca and S. Matarrese, *Imprint of relativistic particles on the anisotropies of the stochastic gravitational-wave background*, *Phys. Rev. D* **103** (2021) 023522 [[2007.01215](#)].

- [119] E. Dimastrogiovanni, M. Fasiello, A. Malhotra, P.D. Meerburg and G. Orlando, *Testing the early universe with anisotropies of the gravitational wave background*, *JCAP* **02** (2022) 040 [[2109.03077](#)].
- [120] LISA COSMOLOGY WORKING GROUP collaboration, *Probing anisotropies of the Stochastic Gravitational Wave Background with LISA*, *JCAP* **11** (2022) 009 [[2201.08782](#)].
- [121] LISA COSMOLOGY WORKING GROUP collaboration, *Cosmology with the Laser Interferometer Space Antenna*, *Living Rev. Rel.* **26** (2023) 5 [[2204.05434](#)].
- [122] C. Ünal, E.D. Kovetz and S.P. Patil, *Multimessenger probes of inflationary fluctuations and primordial black holes*, *Phys. Rev. D* **103** (2021) 063519 [[2008.11184](#)].
- [123] A. Malhotra, E. Dimastrogiovanni, M. Fasiello and M. Shiraishi, *Cross-correlations as a Diagnostic Tool for Primordial Gravitational Waves*, *JCAP* **03** (2021) 088 [[2012.03498](#)].
- [124] Y. Cui, S. Kumar, R. Sundrum and Y. Tsai, *Unraveling Cosmological Anisotropies within Stochastic Gravitational Wave Backgrounds*, [2307.10360](#).
- [125] A. Malhotra, E. Dimastrogiovanni, G. Domènech, M. Fasiello and G. Tasinato, *New universal property of cosmological gravitational wave anisotropies*, *Phys. Rev. D* **107** (2023) 103502 [[2212.10316](#)].
- [126] L. Valbusa Dall’Armi, A. Mierna, S. Matarrese and A. Ricciardone, *Adiabatic or Non-Adiabatic? Unraveling the Nature of Initial Conditions in the Cosmological Gravitational Wave Background*, [2307.11043](#).
- [127] LISA COSMOLOGY WORKING GROUP collaboration, *Primordial black holes and their gravitational-wave signatures*, [2310.19857](#).
- [128] E. Komatsu, *The pursuit of non-gaussian fluctuations in the cosmic microwave background*, Ph.D. thesis, Tohoku U., 2001. [astro-ph/0206039](#).
- [129] PLANCK collaboration, *Planck 2013 Results. XXIV. Constraints on primordial non-Gaussianity*, *Astron. Astrophys.* **571** (2014) A24 [[1303.5084](#)].
- [130] W. Hu, *Angular trispectrum of the CMB*, *Phys. Rev. D* **64** (2001) 083005 [[astro-ph/0105117](#)].
- [131] E. Komatsu, *Hunting for Primordial Non-Gaussianity in the Cosmic Microwave Background*, *Class. Quant. Grav.* **27** (2010) 124010 [[1003.6097](#)].
- [132] N. Kogo and E. Komatsu, *Angular trispectrum of cmb temperature anisotropy from primordial non-gaussianity with the full radiation transfer function*, *Phys. Rev. D* **73** (2006) 083007 [[astro-ph/0602099](#)].
- [133] J. Baker et al., *High angular resolution gravitational wave astronomy*, *Exper. Astron.* **51** (2021) 1441 [[1908.11410](#)].
- [134] J.R. Gair, J.D. Romano and S.R. Taylor, *Mapping gravitational-wave backgrounds of arbitrary polarisation using pulsar timing arrays*, *Phys. Rev. D* **92** (2015) 102003 [[1506.08668](#)].
- [135] J.D. Romano and N.J. Cornish, *Detection methods for stochastic gravitational-wave backgrounds: a unified treatment*, *Living Rev. Rel.* **20** (2017) 2 [[1608.06889](#)].
- [136] LIGO SCIENTIFIC, VIRGO collaboration, *Directional Limits on Persistent Gravitational Waves from Advanced LIGO’s First Observing Run*, *Phys. Rev. Lett.* **118** (2017) 121102 [[1612.02030](#)].

- [137] LIGO SCIENTIFIC, VIRGO collaboration, *Directional limits on persistent gravitational waves using data from Advanced LIGO's first two observing runs*, *Phys. Rev. D* **100** (2019) 062001 [[1903.08844](#)].
- [138] KAGRA, VIRGO, LIGO SCIENTIFIC collaboration, *Search for anisotropic gravitational-wave backgrounds using data from Advanced LIGO and Advanced Virgo's first three observing runs*, *Phys. Rev. D* **104** (2021) 022005 [[2103.08520](#)].
- [139] NANOGrAV collaboration, *The NANOGrav 15 yr Data Set: Search for Anisotropy in the Gravitational-wave Background*, *Astrophys. J. Lett.* **956** (2023) L3 [[2306.16221](#)].
- [140] H. Xu et al., *Searching for the Nano-Hertz Stochastic Gravitational Wave Background with the Chinese Pulsar Timing Array Data Release I*, *Res. Astron. Astrophys.* **23** (2023) 075024 [[2306.16216](#)].
- [141] EPTA, INPTA: collaboration, *The second data release from the European Pulsar Timing Array - III. Search for gravitational wave signals*, *Astron. Astrophys.* **678** (2023) A50 [[2306.16214](#)].
- [142] NANOGrAV collaboration, *The NANOGrav 15-year Data Set: Evidence for a Gravitational-Wave Background*, *Astrophys. J. Lett.* **951** (2023) [[2306.16213](#)].
- [143] D.J. Reardon et al., *Search for an isotropic gravitational-wave background with the Parkes Pulsar Timing Array*, *Astrophys. J. Lett.* **951** (2023) [[2306.16215](#)].
- [144] EPTA collaboration, *The second data release from the European Pulsar Timing Array: V. Implications for massive black holes, dark matter and the early Universe*, [2306.16227](#).
- [145] NANOGrAV collaboration, *The NANOGrav 15-year Data Set: Search for Signals from New Physics*, *Astrophys. J. Lett.* **951** (2023) [[2306.16219](#)].
- [146] G. Franciolini, A. Iovino, Junior., V. Vaskonen and H. Veermae, *The recent gravitational wave observation by pulsar timing arrays and primordial black holes: the importance of non-gaussianities*, [2306.17149](#).
- [147] K. Inomata, K. Kohri and T. Terada, *The Detected Stochastic Gravitational Waves and Subsolar-Mass Primordial Black Holes*, [2306.17834](#).
- [148] Y.-F. Cai, X.-C. He, X. Ma, S.-F. Yan and G.-W. Yuan, *Limits on scalar-induced gravitational waves from the stochastic background by pulsar timing array observations*, [2306.17822](#).
- [149] L. Liu, Z.-C. Chen and Q.-G. Huang, *Implications for the non-Gaussianity of curvature perturbation from pulsar timing arrays*, [2307.01102](#).
- [150] K.T. Abe and Y. Tada, *Translating nano-Hertz gravitational wave background into primordial perturbations taking account of the cosmological QCD phase transition*, [2307.01653](#).
- [151] R. Ebadi, S. Kumar, A. McCune, H. Tai and L.-T. Wang, *Gravitational Waves from Stochastic Scalar Fluctuations*, [2307.01248](#).
- [152] D.G. Figueroa, M. Pieroni, A. Ricciardone and P. Simakachorn, *Cosmological Background Interpretation of Pulsar Timing Array Data*, [2307.02399](#).
- [153] Z. Yi, Q. Gao, Y. Gong, Y. Wang and F. Zhang, *The waveform of the scalar induced gravitational waves in light of Pulsar Timing Array data*, [2307.02467](#).
- [154] E. Mudge, E. Morgante, C. Puchades-Ibáñez, N. Ramberg, W. Ratzinger, S. Schenk et al., *Primordial gravitational waves in the nano-Hertz regime and PTA data – towards solving the GW inverse problem*, [2306.14856](#).

- [155] H. Firouzjahi and A. Talebian, *Induced Gravitational Waves from Ultra Slow-Roll Inflation and Pulsar Timing Arrays Observations*, [2307.03164](#).
- [156] Q.-H. Zhu, Z.-C. Zhao and S. Wang, *Joint implications of BBN, CMB, and PTA Datasets for Scalar-Induced Gravitational Waves of Second and Third orders*, [2307.03095](#).
- [157] Z.-Q. You, Z. Yi and Y. Wu, *Constraints on primordial curvature power spectrum with pulsar timing arrays*, [2307.04419](#).
- [158] G. Ye and A. Silvestri, *Can gravitational wave background feel wiggles in spacetime?*, [2307.05455](#).
- [159] S.A. Hosseini Mansoori, F. Felegray, A. Talebian and M. Sami, *PBHs and GWs from T^2 -inflation and NANOGrav 15-year data*, [2307.06757](#).
- [160] S. Balaji, G. Domènech and G. Franciolini, *Scalar-induced gravitational wave interpretation of PTA data: the role of scalar fluctuation propagation speed*, [2307.08552](#).
- [161] B. Das, N. Jaman and M. Sami, *Gravitational Waves Background (NANOGrav) from Quintessential Inflation*, [2307.12913](#).
- [162] L. Bian, S. Ge, J. Shu, B. Wang, X.-Y. Yang and J. Zong, *Gravitational wave sources for Pulsar Timing Arrays*, [2307.02376](#).
- [163] J.-H. Jin, Z.-C. Chen, Z. Yi, Z.-Q. You, L. Liu and Y. Wu, *Confronting sound speed resonance with pulsar timing arrays*, [2307.08687](#).
- [164] Z.-C. Zhao, Q.-H. Zhu, S. Wang and X. Zhang, *Exploring the Equation of State of the Early Universe: Insights from BBN, CMB, and PTA Observations*, [2307.13574](#).
- [165] L. Liu, Z.-C. Chen and Q.-G. Huang, *Probing the equation of state of the early Universe with pulsar timing arrays*, [2307.14911](#).
- [166] Z. Yi, Z.-Q. You and Y. Wu, *Model-independent reconstruction of the primordial curvature power spectrum from PTA data*, [2308.05632](#).
- [167] L. Frosina and A. Urbano, *On the inflationary interpretation of the nHz gravitational-wave background*, [2308.06915](#).
- [168] S. Choudhury, A. Karde, S. Panda and M. Sami, *Scalar induced gravity waves from ultra slow-roll Galileon inflation*, [2308.09273](#).
- [169] J. Ellis, M. Fairbairn, G. Franciolini, G. Hütsi, A. Iovino, M. Lewicki et al., *What is the source of the PTA GW signal?*, [2308.08546](#).
- [170] M. Kawasaki and K. Murai, *Enhancement of gravitational waves at Q-ball decay including non-linear density perturbations*, [2308.13134](#).
- [171] Z. Yi, Z.-Q. You, Y. Wu, Z.-C. Chen and L. Liu, *Exploring the NANOGrav Signal and Planet-mass Primordial Black Holes through Higgs Inflation*, [2308.14688](#).
- [172] K. Harigaya, K. Inomata and T. Terada, *Induced Gravitational Waves with Kination Era for Recent Pulsar Timing Array Signals*, [2309.00228](#).
- [173] H. An, B. Su, H. Tai, L.-T. Wang and C. Yang, *Phase transition during inflation and the gravitational wave signal at pulsar timing arrays*, [2308.00070](#).
- [174] M.R. Gangopadhyay, V.V. Godithi, K. Ichiki, R. Inui, T. Kajino, A. Manusankar et al., *Is NanoGRAV signals pointing towards resonant particle creation during inflation?*, [2309.03101](#).

- [175] Z. Chang, Y.-T. Kuang, D. Wu and J.-Z. Zhou, *Scalar Induced Gravitational Waves from Finslerian Inflation and Pulsar Timing Arrays Observations*, [2309.06676](#).
- [176] K. Inomata, M. Kawasaki, K. Mukaida and T.T. Yanagida, *Axion Curvaton Model for the Gravitational Waves Observed by Pulsar Timing Arrays*, [2309.11398](#).
- [177] S. Choudhury, K. Dey, A. Karde, S. Panda and M. Sami, *Primordial non-Gaussianity as a saviour for PBH overproduction in SIGWs generated by Pulsar Timing Arrays for Galileon inflation*, [2310.11034](#).
- [178] S. Choudhury, K. Dey and A. Karde, *Untangling PBH overproduction in w -SIGWs generated by Pulsar Timing Arrays for MST-EFT of single field inflation*, [2311.15065](#).
- [179] G. Domènech, *Cosmological Gravitational Waves from Isocurvature Fluctuations*, [2311.02065](#).
- [180] Z. Chang, Y.-T. Kuang, D. Wu, J.-Z. Zhou and Q.-H. Zhu, *New constraints on primordial non-Gaussianity from missing two-loop contributions of scalar induced gravitational waves*, [2311.05102](#).
- [181] B. Mu, J. Liu, G. Cheng and Z.-K. Guo, *Constraints on ultra-slow-roll inflation with the NANOGrav 15-Year Dataset*, [2310.20564](#).
- [182] S. Choudhury, A. Karde, S. Panda and M. Sami, *Realisation of the ultra-slow roll phase in Galileon inflation and PBH overproduction*, [2401.10925](#).
- [183] Z.-C. Chen and L. Liu, *Can we distinguish the adiabatic fluctuations and isocurvature fluctuations with pulsar timing arrays?*, [2402.16781](#).
- [184] LIGO SCIENTIFIC, VIRGO collaboration, *GWTC-1: A Gravitational-Wave Transient Catalog of Compact Binary Mergers Observed by LIGO and Virgo during the First and Second Observing Runs*, *Phys. Rev. X* **9** (2019) 031040 [[1811.12907](#)].
- [185] LIGO SCIENTIFIC, VIRGO collaboration, *GWTC-2: Compact Binary Coalescences Observed by LIGO and Virgo During the First Half of the Third Observing Run*, *Phys. Rev. X* **11** (2021) 021053 [[2010.14527](#)].
- [186] LIGO SCIENTIFIC, VIRGO, KAGRA collaboration, *GWTC-3: Compact Binary Coalescences Observed by LIGO and Virgo During the Second Part of the Third Observing Run*, [2111.03606](#).
- [187] X. Wang, Y.-l. Zhang, R. Kimura and M. Yamaguchi, *Reconstruction of power spectrum of primordial curvature perturbations on small scales from primordial black hole binaries scenario of LIGO/VIRGO detection*, *Sci. China Phys. Mech. Astron.* **66** (2023) 260462 [[2209.12911](#)].
- [188] G. Domènech and M. Sasaki, *Probing Primordial Black Hole Scenarios with Terrestrial Gravitational Wave Detectors*, [2401.07615](#).
- [189] T. Papanikolaou, X.-C. He, X.-H. Ma, Y.-F. Cai, E.N. Saridakis and M. Sasaki, *New probe of non-Gaussianities with primordial black hole induced gravitational waves*, [2403.00660](#).
- [190] S. Young and C.T. Byrnes, *Signatures of non-gaussianity in the isocurvature modes of primordial black hole dark matter*, *JCAP* **04** (2015) 034 [[1503.01505](#)].
- [191] PLANCK collaboration, *Planck 2018 results. X. Constraints on inflation*, *Astron. Astrophys.* **641** (2020) A10 [[1807.06211](#)].